

Idealising mesh modelling for haptic enabled services and operands

E. Govea-Valladares^{1*}, H. I. Medellin-Castillo¹, C. Fletcher², T. Lim², J. Ritchie², Xiu-Tian Yan³, Victor Arnez⁴ and Ernesto Hernandez⁴

¹ Facultad de Ingeniería, Universidad Autónoma de San Luis Potosí, S.L.P. México

² Innovative Manufacturing Research Centre, Heriot-Watt University, Edinburgh, UK

³ Design, Manufacture & Engineering Management, University of Strathclyde, Glasgow, UK

⁴ Facultad de Ingeniería, Universidad Nacional Autónoma de México, D.F. México

* Corresponding author: eder.govea@gmail.com

Abstract. Communicating the knowledge and science of product engineering, analysis and manufacturing planning is an area of continued research driven by the digital economy. Virtual Reality (VR) is a generally accepted interactive digital platform which industry and academia have used to model engineering workspaces. Interactive services that generate a sense of immersion, particularly the sense of touch to communicate shape modelling and manipulation, is increasingly being used in applications that range from Design For Manufacturing and Assembly (DFMA) and Process Planning (PP) to medical applications such as surgical planning and training. In simulation, the natural way for solid modelling is the use of primitive geometries, and combinations of them where complex shapes are required, to create, modify or manipulate models. However, this natural way makes use of Booleans operands that require large computational times which make them inappropriate for real time VR applications. This work presents an insight on new methods for haptic shape modelling focused on Boolean operands on a polygon mesh. This is not meant as a contrast to point/mesh-editing methods, instead it is focused on idealising polygonal mesh modelling and manipulation for use with haptics. The resulting models retain a high level of geometric detail for visualisation, modelling, manipulation and haptic rendering.

Keywords: Mesh modelling, Boolean operations, Haptic rendering, Process Planning.

1. Introduction

Through the years, computer simulation has been a tool used to model real life situations by using a computer program. Traditionally, system modelling uses a mathematical model, which attempts to find analytical solutions to problems, trying to predict the behaviour of a system [1]. There are many different types of computer simulations; the common feature that they all share is the attempt to generate a sample of representative scenarios for a model and its behaviour [2].

Object modelling is a tool used in mechanical engineering to design parts [3]. Simulations play an important role in the product design process, reducing the

need for expensive prototyping and reducing the product development cost [4]. Most of commercial modelling software focuses on the visual editing, but when haptics is added the user experience through tactile engagement is superior. Precision and accuracy are desired characteristics in these systems, but it is directly dependent on the computational capabilities and the data size and complexity. The more data, the more specific becomes the model [5]. The time performance of the modelling and simulation process is a current subject under study. Current methods such as performing Boolean Operations on Polygon Meshes and implicit functions [6] are usually very slow.

This paper presents a new algorithm developed for mesh modelling and manipulation with haptics. Union, intersection and difference Boolean operands are ‘localised’ to the contact area between the two objects to speed up processing to move closer to a real-time performance. The implementation is done in VTK [7] with collision libraries of VTKBioEng [8] programmed in C++.

2. Related Work

The editing and manipulation of 3D models has seen constant research activity particularly in the area of CAD. Several techniques relevant for physics-based simulations are listed in [7]. In this work the modelling techniques for fully-automatic or semi-automatic simplification of CAD models are also characterized. In [8] a set of interactive free-form editing operators for direct manipulation of level-set models to support the creation and removal of surface detailed by operators for volumetric implicit surfaces is presented.

3D modelling with triangular mesh has become increasingly popular in engineering where fast

modifications of the mesh models means critical problems can be solved quickly without going back to the CAD model. An algorithm that removes the intersecting faces in an n-ring neighbourhood is presented in [9]. The algorithm produces triangles whose sizes smoothly evolve according to the possibly heterogeneous sizes of the surrounding triangles. Regarding the formation of new models from primitive objects, techniques for rendering implicit surfaces using point based primitives were presented in [10]. A method for real time modelling was presented in [11], where a modelling approach using signed distance functions for objects and complex surface manipulations with immediate visual feedback was described. A new method for implicit modelling was presented in [12]. It was proposed a method to describe sharp features (edges and vertices) applying a new surface modelling representation.

In [13] Boolean operations to construct heterogeneous material objects were introduced. Boolean operations use Boolean algebra to model more complex objects. The operands of addition, subtraction and common are used in this modelling technique [14]. Boolean modelling can be readily implemented in CAD/CAE/CAM software. An algorithm to calculate intersection, union and difference was proposed in [15]. The algorithm is valid for general planar polygons based on algebraic operations to calculate the intersection between general polygons. Similarly, an algorithm for Boolean operations on polyhedral solid representations using approximate arithmetic was described in [16].

Haptic editing of 3D models was presented in [17], where the integration of Virtual Reality (VR) and Computer-Aided Design (CAD) was investigated. The proposed system made possible the intuitive and direct 3D edition of CAD objects through B-Rep modelling in CATIA and haptic aided by grid and extrude commands. Some commercial haptics 3D modellers are based on point clouds that define surfaces, essentially for applications of sculpture or artistic modelling. For example, the Splodge software of Sensable [18] or the Cre8 of Novint [20] allow 3D modelling of objects in real time.

From the literature review, it can be concluded that simulation with mesh models, haptic fast edition and manipulation of the 3D models using open source libraries and multi haptic devices, is not an area that has been explored by researchers. The purpose of this work is to model 3D mesh objects via a haptic interface and using enhanced Boolean operations. The proposed method is based on dividing the main piece (Object 1) into regions and manipulates the haptic cursor or tool (Object 2) to modify the main piece and create a new model. The aim of the method is the optimization of the processing speed when a Boolean operation is applied.

3. Methodology

Figure 1 presents the proposed methodology for haptic modelling using localised Boolean. This methodology has been implemented using C++, Visualization Toolkit libraries (VTK 5.6.1), and collision detection with VKTBioEng v5.0.1. Open Source Haptics H3D v2.1.1 is also used for haptic rendering, which in this case is carried out by the Phantom Omni from Sensable and the Falcon from Novint haptic devices. The system has been implemented in a PC with a 1.73 GHz processor, 2.0GB of RAM and Windows XP.

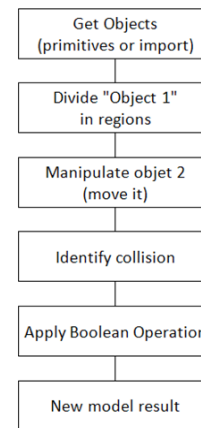


Fig. 1. Proposed Boolean localised methodology

1. - Get objects: The modelling process start with the definition of the objects in the scene (objects 1 and object 2). These objects can be created with VTK libraries (primitives) or imported from CAD systems as STL files.

2. - Divide “Object 1” in regions: In this step Object 1 is divided into smaller parts and named with an ID for identification. The algorithm divides the mesh using a filter that separates the cells of a dataset into spatially aggregated pieces using an Oriented Bounding Box (OBB) method. The division can be done by specifying the number of elements or the number of points in one area.

3. - Manipulate “Object 2”: Object 2 can be either the haptic cursor or an object being controlled with the haptic cursor. Object 1 and 2 must be in contact to allow Boolean operand being used.

4. - Identify collision: The algorithm takes only the regions of object 1 that are in contact with object 2 and creates a “polydata” variable. The data like points and elements of these regions can be extracted. The elements that are not in contact with the cursor will not be selected and will not be included in the Boolean operation procedure.

5. - Apply Boolean operation: The selected “polydata” is sent to the Boolean operation function to perform Union, Intersection or Difference.

6. - New model result: Once the Boolean operand has been done, the new section will be added to object 1.

Figure 2 shows an example of Object 1 after being divided into regions (colors) and the object 2 (white sphere) being the haptic cursor, before the Boolean operation.

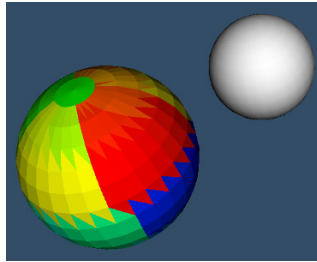


Fig.2 Objects for the haptic modelling

4. Implementation

Four case studies were selected to test and evaluate the proposed localised approach to perform Boolean operands (intersection, union and difference) in virtual haptic modelling. For comparison purposes, Boolean operations were applied to these case studies using both, the proposed and the conventional, Boolean methods.

Case 1: Two primitive objects with regular curved surfaces (spheres) were used. Each comprises a mesh size of 780 elements. The results of each Boolean operand are shown in Fig. 3.

Case 2: In this case, a primitive cube comprising 12 triangular elements, and a sphere cursor with 780 elements were selected. The purpose of this case was to observe the behaviour of the Boolean operations when applied to an object with low resolution. Fig. 4 shows the results of the Boolean operands.

Case 3: A more complex model i.e., a gear with 1767 triangular elements was used. The objective is to test the response of the Boolean operands in areas with elements of different sizes. Fig. 5 shows the results.

Case 4: The last case study is shown in Fig. 6. A jaw model with 9230 elements and spherical cursor were selected. The objective is to assess the performance of Boolean operands in high-resolution models of irregular geometry.

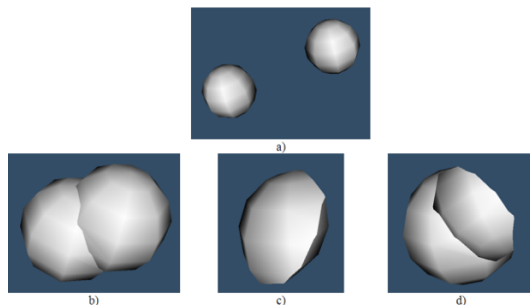


Fig. 3 Objects for the case 1: (a) source objects, (b) union, (c) intersection and (d) difference.

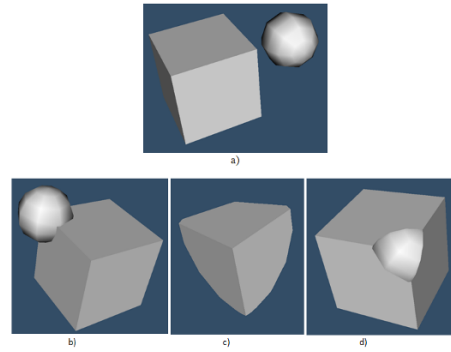


Fig. 4 The regular cube and cursor: (a) source objects, (b) union, (c) intersection and (d) difference.

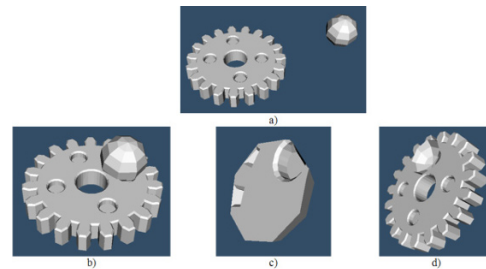


Fig. 5 Gear and tool for the case study 3: (a) source objects, (b) union, (c) intersection and (d) difference.

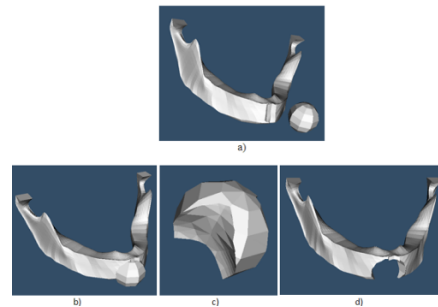


Fig. 6 High resolution jaw and cursor: (a) source objects, (b) union, (c) intersection and (d) difference.

5. Results

In order to compare the time performance of the two Boolean methods, localised and conventional, processing time was measured using the CPU processor clock. Table 1 present the time performance results of the Boolean operands using the conventional approach, whilst Table 2 shows the time performance results using the proposed localised based approach. Each Boolean operand was applied ten times to each case study; the results reported in Table 1 and 2 correspond to the average values of each test.

From the results presented in Table 1 and 2 it can be observed that the proposed localised Boolean approach is approximately 25% faster than the conventional Boolean approach. This is due to the fact that the proposed

approach uses less data (localised data) than the conventional approach where the whole mesh is used in the Boolean operand. Since the proposed algorithm separates into parts the complete mesh of each object and uses a collision detection filter to localise and select the area of interest, the time performance is improved. By enabling discreet haptic region selection, only the elements and associated vertices of the selected regions will be affected, thus avoiding the need of processing the whole mesh.

It can be observed that as the number of elements of the mesh models increases (more complex models), the processing time increases. The quality of the models was not affected when using the localised proposed method.

Table 1. Conventional Boolean operation, milliseconds

Haptic cursor with	UNION	INTERSECTION	DIFFERENCE
Sphere	5.715	5.766	4.422
Cube	4.922	4.798	4.098
Gear	6.948	6.630	5.778
Jaw	7.896	7.577	7.487

Table 2. Localised Boolean operation, milliseconds

Haptic cursor with	UNION	INTERSECTION	DIFFERENCE
Sphere	4.458	4.497	3.449
Cube	3.741	3.646	3.114
Gear	5.211	4.973	4.334
Jaw	5.685	5.455	5.391

6. Conclusions and future work

A new method to improve the time performance of Boolean operands has been proposed. The proposed method is based on a collision detection approach to localise contact areas. It has been proved that by 'localising' a Boolean operand on mesh models, it is possible to reduce the execution time compared with Boolean conventional operations that do not discriminate elements. It has to be mentioned that in haptic virtual reality systems, haptic rendering may be slower than Boolean operands and therefore the simulation may not be perform in real-time. Future work considers the optimization of haptic virtual reality applications using the proposed Boolean operations approach based on localised collisions.

Acknowledgements: The authors wish to thank to Consejo Nacional de Ciencia y Tecnología (CONACyT), Universidad Autónoma de San Luis Potosí (UASLP) and Heriot-Watt University (HWU) for the invaluable support to carry out this research work.

References

- [1] Oliver Rübél, Sean Ahern, E. Wes Bethel, Mark D. Biggin, Hank Childs, Estelle Cormier-Michel, Angela DePace, Michael B. Eisen, Charles C. Fowlkes, Cameron G. R. Geddes, Hans Hagen, Bernd Hamanna, Min-Yu Huang, Soile V. E. Keränen, David W. Knowles, Cris L. Luengo Hendriks, Jitendra Malik, Jeremy Meredith, Peter Messmere, Prabhat, Daniela Ushizima, Gunther H. Weber, Kesheng Wu. "Coupling visualization and data analysis for knowledge discovery from multi-dimensional scientific data", *Procedia Computer 1* (2010) 1757-1764.
- [2] ChaoliWang and Han-Wei Shen, "Information Theory in Scientific Visualization", *Entropy 13* (2011), 254-273
- [3] Junji Nomura, Kazuya Sawada. "Virtual Reality Technology and its Industrial Applications", *Annual Reviews In Control 25* (2001) 99-109
- [4] Jesús David Cardona, Miguén Ángel Hidalgo, Héctor Castán, Fabio Rojas, Diego Borro, Héctor Jaramillo, "Realidad Virtual y Procesos de Manufactura" ISBN 978-958-8122-51-9. (2007) Colombia, primera edición.
- [5] Atul Thakur, Ashis Gopal Banerjee, Satyandra K. Gupta. "A survey of CAD model simplification techniques for physics-based simulation applications. *Computer-Aided Design 41* (2009) 65-80
- [6] H. Masuda, "Topological operators and Boolean operations for complex-based nonmanifold geometric models", *Computer-Aided Design 2* (1993) 119 - 129.
- [7] VTK - The Visualization Toolkit, <http://www.vtk.org/>
- [8] Vtkbioeng, <http://www.bioengineering-research.com/>
- [9] Atul Thakur, Ashis Gopal Banerjee, Satyandra K. Gupta. "A survey of CAD model simplification techniques for physics-based simulation applications", *Computer-Aided Design 41* (2009) 65-80
- [10] Manolya Eyiurekli, David Breen, "Interactive free-form level-set surface-editing operators", *Computers & Graphics 34* (2010) 621-638
- [11] Ruding Loua, Jean-Philippe Pernot, Alexei Mikchevitch, Philippe Vérona, "Merging enriched Finite Element triangle meshes for fast prototyping of alternate solutions in the context of industrial maintenance", *Computer-Aided Design 42* (2010) 670-681
- [12] Emilio Vital Brazil, Ives Macedo, Mario Costa Sousa, Luiz Velho, Luiz Henrique de Figueiredo, "Shape and tonedepictionforimplicitsurfaces", *Computers & Graphics 35* (2011) 43-53
- [13] Tim Reiner, Gregor Muckl, Carsten Dachsbacher, "Interactive modeling of implicit surfaces using a direct visualization approach with signed distance functions", *Computers & Graphics 35*(2011) 596-603
- [14] Xinghua Song, Bert Juttler, "Modeling and 3D object reconstruction by implicitly defined surfaces with sharp features", *Computers & Graphics 33* (2009) 321-330
- [15] W. Sun, X. Hu, "Reasoning Boolean operation based modeling for heterogeneous objects", *Computer-Aided Design 34* (2002) 481-488
- [16] M. Rivero, F.R. Feito, "Boolean operations on general planar polygons", *Computers & Graphics 24* (2000) 881-896
- [17] J.M. Smith, N.A. Dodgson, "A topologically robust algorithm for Boolean operations on polyhedral shapes using approximate arithmetic", *Computer-Aided Design 39* (2007) 149-163
- [18] P. Bourdot, T. Convard, F. Picon, M. Ammi, D. Touraine, J.-M. Vézien, "VR-CAD integration: Multimodal immersive interaction and advanced haptic paradigms for implicit edition of CAD models", *Computer-Aided Design 42* (2010) 445-461
- [19] Sensable, <http://www.sensable.com/>
- [20] Novint, <http://www.novint.com/>

Analysis of dynamic properties of a multi-stage gear system using the flexible multi-body system modelling technique

M. Sulitka¹, Z. Neusser² and J. Veselý¹

¹ Research Center for Manufacturing Technology, Czech Technical University in Prague, Faculty of Mechanical Engineering, Horská 3, Praha 2, 128 00, Czech Republic

² Department of Mechanics, Biomechanics and Mechatronics, Czech Technical University in Prague, Faculty of Mechanical Engineering, Technická 4, Praha 6, 166 07, Czech Republic

Abstract. The paper presents a model of a tooth gear system which allows a complex analysis of dynamic properties of the feed drive. The model, comprising a description of shaft, bearings, wheel and gearbox compliances, is assembled in state space as a coupled system of finite element models and includes a description of the stiffness of tooth contact. A measurement for verification of the proposed model is done using a single gearbox unit, as well as the entire system of a machine tool feed drive.

Keywords: Tooth gear system, Feed drive model, Machine tool

1. Introduction

The development of big machine tools with large working ranges has been intensively expanding, using rack-pinion feed drive systems increasingly as a substitute of common ball screw drives. A suitable choice of feed drive mechanism is closely linked to the interaction between the feed drive and the structure of the machine tool. An effectively optimised feed drive design can be achieved by using coupled models combining the description of feed drive and machine tool frame.

A model of a multistage tooth gear system derived from a discrete description is shown e.g. in [1]. In the present paper, a FE-based model is introduced which was developed for application in machine tool feed drive simulations. In addition to a detailed description of tooth contact and the compliance of the mechanical structure of the gear system, special attention has been paid to the contact between shaft, key and wheel.

2. Gear system model

For simulations of dynamic properties of the gear system both in frequency and time domain, a model was created which includes a description of all the important elements

of the mechanical gear system including tooth contact, shaft and wheel mechanics, bearings and gear box.

2.1. Tooth contact model

The tooth contact model assumes an ideal contact of a wheel couple. Calculation of the contact uses a modified Hertz theory [2], using the more precise parameters of tooth tilting derived in [3] and tooth bending in [4] (see Fig. 1). The resulting force is dependant on the load of the coupled gears and the rotation, with a different number of teeth in contact. Stiffness used to substitute tooth contact has been calculated as an average of instantaneous flexibilities. Dynamic properties of the tooth contact model and comparison with measurements introduces [5].

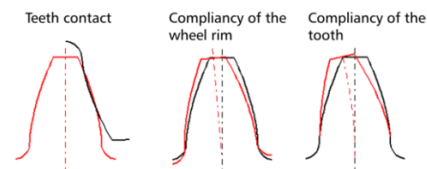


Fig. 1. Components of the compliance of tooth contact

2.2. Contact stiffness

The calculation of the stiffness of the gear contact is based on the two tooth penetration formula, in which the total penetration is dependant on the bending of both teeth caused by contact force F_N , the tilting of both teeth and the transformations of the sides of the teeth in contact, according to formula 1.

$$\delta = F_N g_{tilting1} + F_N g_{bending1} + F_N g_{contact}(F_N) + F_N g_{tilting2} + F_N g_{bending2} \quad (1)$$

Compliances g_x are dependant on the line of contact, tooth profile and material properties of the gears. Variable $g_{contact}$ is described in a non-linear dependence featuring contact force F_N . Therefore, the formula (1) must be solved iteratively. The stiffness of the contact is determined by dividing the contact force with total penetration.

2.3. Shaft and wheel model

An important component of the overall compliance of the gear system is represented by the system of shafts and wheels. A model was designed, enabling simulations of the operation of the gear system over time and the creation of the machine tool feed drive coupled models. An FE model, including the contact problem between shaft, key and wheel, is used for the calculation of static analysis, delivering the stiffness k_{CS} [N/m] between a wheel W on which a tangent force F is applied and a pinion P, fixed on the circumference by the tooth contact line (Fig. 2). The shaft is fixed in bearing locations.

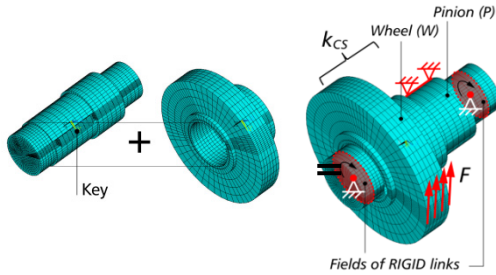


Fig. 2. The FE model of the shaft and wheel for a static analysis with the shaft, key and wheel contact problem.

This type of model, however, cannot be used for efficient simulations in time domain. For this reason, another FE model was created, where the shaft is united with the wheels.

Through modal decomposition, this model is transformed into state space with interface nodes i, j, k, l selected to define the force inputs and outputs of positions and rotations at points, representing the bearings and wheels (Fig. 3). This model can then be used to determine the torsion stiffness k_{SS} [Nm/rad] between the wheel W and pinion P.

2.4. Coupled shaft and gearbox model

The coupling of the shaft models with the wheels and the gearbox is carried out in state space (Fig. 4). The coupling force between the shaft wheels 1 and 2 is determined using the total stiffness of one wheel pair

$$k_{12} = \frac{1}{\frac{1}{k_t} + \frac{1}{k_{CS}} - \frac{r_W^2}{k_{SS}}} \text{ [N/m]}, \quad (2)$$

where k_t [N/m] is the contact stiffness derived from (1) and k_{CS} [N/m] is the stiffness between the wheel and the pinion of the FE model considering the contact between shaft, key and wheel (Fig. 2). Subtracted is the element with the torsion stiffness k_{SS} [Nm/rad], transformed to its axial representation using the wheel radius r_w . On interface nodes j, k (Fig. 4), there is a torque of

$$M_{1,2} = k_{12}(r_1\varphi_1 + r_2\varphi_2)r_{1,2}^2 \quad (3)$$

where φ is the rotation of the teeth and r is the appropriate gear diameter.

To determine the coupling force between the shaft and the gearbox, the stiffness values of the bearings are used.

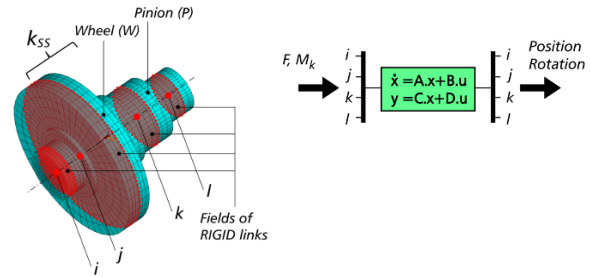


Fig. 3. A full FE model of the shaft with wheels for export in state space (a schematic is shown on the right)

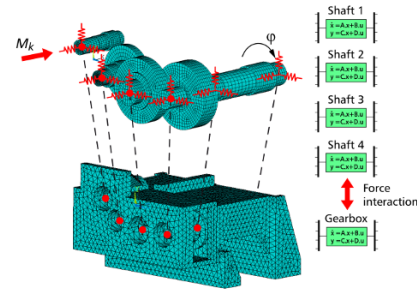


Fig. 4. Coupled model of shaft with wheels and the gearbox

3. Measuring the stiffness of the gear system

The stiffness of the pinion's mesh with the rack and the overall stiffness of the gear system is determined via measuring on a multifunctional test bench. The considered gear system has three stages, straight teeth and a pinion on the output shaft meshing with a diagonal-toothed rack. The kinematic path of the gear system corresponds to the model in Fig. 4.

The arrangement of the test bench and tested gear system for the measurement can be seen in Fig. 5. In addition to the rotation (1) on the input shaft, rotation (2) on the output pinion and the torque on the input, deviations of the gearbox relative to the rack were also measured in directions X , Y and Z .

The gear system has been loaded by a controlled alternating torque of the servomotor, with three selected amplitude levels of the load torque. The information from rotation sensors φ_1 , φ_2 and torque M_k on the output shaft are used to determine the overall stiffness of the gear system relative to the input as,

$$k_T = \frac{\varphi_1 - p_R(\varphi_2 - \Delta\varphi_2)}{M_k}, \quad (4)$$

where p_R is the overall transmission. For the additional rotation of the pinion $\Delta\varphi_2$ caused by the gearbox being moved relative to the rack because of the compliance of the consoles, the following can be derived:

$$\Delta\varphi_2 = \frac{\Delta y \cdot \tan(\beta) \cdot \cos(\alpha)}{r_b}, \quad (5)$$

where α is the angle of the sides of the rack's teeth, β the angle of the teeth and r_b is the radius of the pitch circle of the pinion.

The measurements are used to derive not only the stiffness of the entire transmission system, but also of the pinion's mesh with the rack.

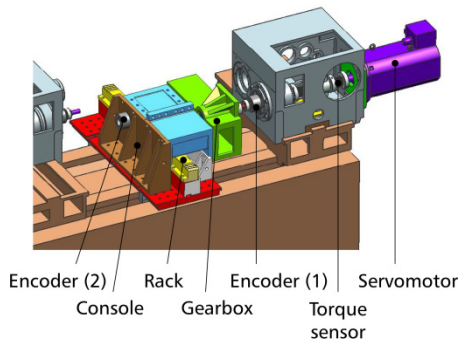


Fig. 5. Picture of gear system measuring arrangement

4. Verification of the gear system stiffness

Hysteresis loops of the dependence of load torque on rotation are determined from the measurements, with an example of shown in Fig. 6.

In the range of used torque amplitudes, stiffness values have been determined which correspond to central lines of the hysteresis loops, with a range of 300 to 500 Nm/rad (). These points at obviously non-linear characteristic of the gear system. The simulation model evaluates linearised stiffness values, which are compared

with the measured ones in the chart in Fig. 7. Well match of the model with measurements can be seen.

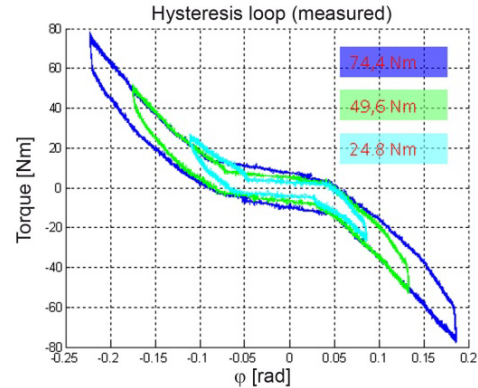


Fig. 6. Measured hysteresis loops of the gear system

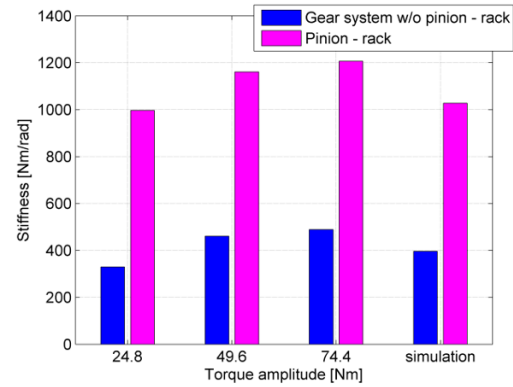


Fig. 7. Stiffness of the gear system relative to input. Comparison of the measurements and simulation

5. Verification of the feed drive model of the machine tool motion axis

The tested gear system is used on a large portal vertical milling machine as a feed unit of the X motion axis. For the analysis of the feed drive dynamic properties, a coupled model of the drive of X axis is created, including an FE model of the machine tool structure and a simplified two-mass substitution of the gear system mechanics. The gear system simplified model uses the value of the overall torsion stiffness determined using the detailed model described above.

5.1. Feed drive coupled model

A coupled model of the feed drive and machine tool structure is created using the procedure described e.g. in [6], [7]. The machine tool structure is modelled by FE and using the modal decomposition method, the FE

model is transformed into state space. A schematic picture of the model is shown in Fig. 8.

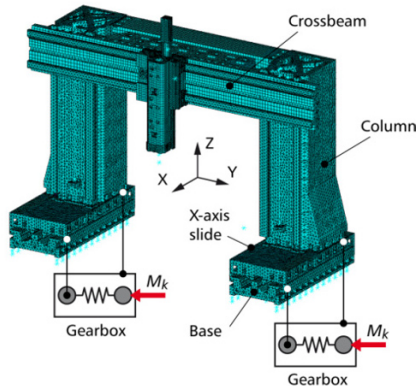


Fig. 8. FE model of the machine and the connection with simplified models of the X-axis gear system

6. Feed drive dynamic properties

Dynamic properties of the feed drive mechanical structure are expressed with the frequency transfer φ_M/x_L between the rotation of motor φ_M (encoder) and a linear movement of the column x_L (linear ruler). This transfer can be evaluated with a combination of functions φ_M/M_k and x_L/M_k

$$G_{ML} = \frac{\varphi_M}{x_L} = \frac{\varphi_M}{M_k} \cdot \frac{M_k}{x_L} = \frac{\varphi_M}{M_k} \cdot \left(\frac{x_L}{M_k}\right)^{-1} \quad (6)$$

A comparison between the measured and simulated characteristics is shown in a chart in Fig. 9. It can be seen that the simulation corresponds to the measurements very well, both in frequency and amplitude. It is particularly important to note the very good correspondence of the value of the first anti-resonance frequency at the first point the characteristic's amplitude drops.

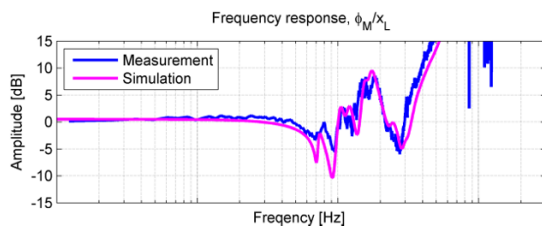


Fig. 9. Frequency transfer of the machine's feed drive. Comparison of measurements and simulation

Regulation theory [8] has proven that setting of the position control loop gain is limited primarily by the first anti-resonance frequency. In addition to this value, however, there are also higher natural frequencies and

their oscillation amplitudes entering the feed drive control dynamics, and the model shows very good correspondence with the measurements in this area as well. The resulting model can thus be beneficially used for relevant simulations of feed drive control dynamics.

7. Summary

A detailed model of a gear system was created, including a description of the stiffness of the teeth mesh, the transmission path and the gearbox. The model is designed as a flexible multi-body system, enabling time and frequency domain simulations. The proposed shaft modelling approach also considers the contact of the shaft – key – wheel system. The model is verified with measurements on a real gear system using a specialised testing bench, determining a very good correspondence between the simulated and measured values. The gear system model is also verified on a real machine tool motion axis. The model shows a very good correspondence with the real dynamic properties of the feed drive and therefore it can well be applied in machine tool feed drive coupled models for simulating and optimizing the feed drive control dynamics.

Acknowledgements: This research has been supported by the 1M0507 grant of the Ministry of Education of the Czech Republic.

References

- [1] Tanaka E, Tanaka N, Ohno k, (2001) Vibration analysis of a multi-stage gear system including drive mechanism elements. JSME Int Journal, Ser C. Mech Systems, Mach Elem Manuf, Vol. 44, No. 2
- [2] Petersen D, (1989) Auswirkung der Lastverteilung auf die Zahnfußtragfähigkeit von hoch überdeckenden Strinradpaarungen. Dissertation, Hamburg, Germany
- [3] Sainsot P, Vex P. (2004) Contribution of Gear Body to Tooth Deflections - A New Bi-dimensional Analytical Formula. Journal of Mechanical Design, Vol. 126: 748-752
- [4] Weber C, Banaschek K, (1953) Formänderung und Profilrücknahme bei Gerad-und Schrägverzahnten Rädern. Heft 11, F. Vieweg und Sohn, Braunschweig, Germany.
- [5] Neusser Z, Sopouch M, Schaffner T, Pribsch H-H, (2010) Multi-body Dynamics Based Gear Mesh Models for Prediction of Gear Dynamics and Transmission Error. SAE conference, Detroit, USA.
- [6] Sulitka M, Strakoš P, (2007) Complex model of a real machine tool feed drive axis with ball screw. Conference VIDA 2007; Poznan, Poland,
- [7] Vesely J, Sulitka, M, (2008) Machine Tool Virtual Model. International Congress MATAR 2008, Part 1: Drives & Control, Design, Models & Simulation; Prague; Czech Republic;
- [8] Souček, P, (2004) Servomechanism in machine tools (in Czech). CTU of Prague, Praha.

An efficient offline method for determining the thermally sensitive points of a machine tool structure

N. S. Mian, S. Fletcher, A. P. Longstaff and A. Myers
University of Huddersfield, Queensgate, HD1 3DH, UK

Abstract. Whether from internal sources or arising from environmental sources, thermal error in most machine tools is inexorable. Out of several thermal error control methods, electronic compensation can be an easy-to-implement and cost effective solution. However, analytically locating the optimal thermally sensitive points within the machine structure for compensation have been a challenging task. This is especially true when complex structural deformations arising from the heat generated internally as well as long term environmental temperature fluctuations can only be controlled with a limited number of temperature inputs. This paper presents some case study results confirming the sensitivity to sensor location and a new efficient offline method for determining localized thermally sensitive points within the machine structure using finite element method (FEA) and Matlab software. Compared to the empirical and complex analytical methods, this software based method allows efficient and rapid optimization for detecting the most effective location(s) including practicality of installation. These sensitive points will contribute to the development and enhancement of new and existing thermal error compensation models respectively by updating them with the location information. The method is shown to provide significant benefits in the correlation of a simple thermal control model and comments are made on the efficiency with which this method could be practically applied.

Keywords: Finite element analysis, FEA, Matlab, Thermal error, Thermal error compensation, Thermally sensitive locations.

1. Introduction

Thermal errors have been identified as a major contributor to the overall volumetric error of a machine tool, in many cases up to 70% [1]. Several techniques based on analytical, empirical and numerical methods have been established to control the effect of thermal errors. These techniques are widely used and applied with a basic ideology to establish a thermal model based on relationships between the measured temperature of the machine from various locations, used as temperature inputs and the displacement at the tool [2]. The temperature inputs however in some cases may be difficult to identify if propagation of the temperature gradients is complex due to the combined effect of internal and external heat sources and perhaps due to the

complexity of the machine structure. These ambiguities therefore add complexities to identify sensitive locations within the structure and stand out to be a challenging task with a limited number of temperature inputs. It has been observed that the performance of the conventional empirical and statistical approaches such as Artificial Neural Network (ANN) and Linear Regression [3, 4] heavily rely on the data from sensitive location within the machine structure for effective and robust thermal compensation such as varying environmental conditions. Kang et al. [5] used a hybrid model consisting of regression and NN techniques to estimate thermal deformation in a machine tool. The total of 28 temperature sensors were placed on (18) and around (10) the machine to acquire internal heating and environmental data. The training time for the model was 3 hours. Yang et al. [6] tested INDEX-G200 turning centre to model thermal errors. Temperature variables were selected using engineering judgement as temperature sensors were placed on or near the possible heat sources and Multiple Linear Regression technique was used to model thermal errors. Training time for the thermal model however was not mentioned. Krulewich [7] used the Gaussian integration method using polynomial fit to identify the optimum thermal points on the machine spindle. The spindle was put through heating and cooling cycles providing 3.5 hours of training data to locate three optimum measurement points where the results correlated to 96%. The author compared this method with a statistical technique and found that the Gaussian integration method requires significantly less training data.

It has been observed that a significant amount of data is generally required to identify sensor locations and train models which inevitably require machine downtime; therefore, such methodologies can be impractical for general application. It is also the fact that machine structures are sensitive to environmental changes which means that the training data acquired in the first instance may not respond well to the new conditions and therefore a new set of training data may be required [7]. This paper

presents an offline technique based on FEA. The technique provides the ability to identify optimised sensitive locations within the machine structure offline for any set of data either from internal heating or external environmental conditions. Being software based, using the Graphical User Interface (GUI) of the FEA software, this technique integrates the visual aspect to aid reviewing the location of the sensitive areas and the practicality for sensor installations. The application of this technique requires minimal machine downtime as any set of the measured thermal conditions can be assessed offline to obtain the thermal behaviour of the machine. This means that new sensitive areas inside the machine structure may be located according to the new thermal conditions. Satisfactory correlations between the measured and the FEA simulated results are a prerequisite to the application of this technique. In this paper, this technique is applied on the results from simulation case study previously conducted.

2. Case Study

This study was conducted on a 3 axis Vertical Machining Centre (VMC) located on the shop floor with uncontrolled environmental temperature. The FEA model of machine was created in Abaqus/Standard 6.7-1 software [10] using manufacturer provided engineering drawings. Fig. 1 shows the generated CAD model of the machine. The model of the machine was simplified by cutting into half because of the symmetry in the X axis direction and complex structures such as fillets and chamfers were simplified and represented using simple corners to avoid complexity of meshing and nodes.

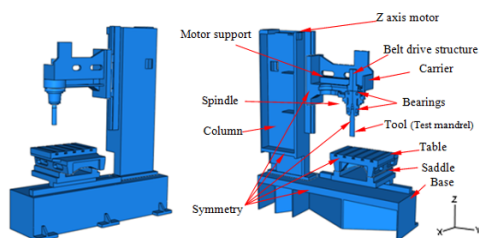


Fig. 1. Generated CAD model of the machine assembly

Mian et al. [8, 9] conducted tests to exploit the thermal behaviour of the VMC when subjected to the spindle heating and varying environmental conditions. Mian et al. [8, 9] proposed a technique in which only one short term data set obtained during one hour internal heating is required to obtain thermal parameters and simulate the heat transfer within structures. This short term data set is used to create the FEA thermal model to simulate the machine for a variety of real world testing regimes. The results showed good correlation between the experimental results and the FEA simulated results typically between 70% and 80%. Mian et al. [9] also conducted environmental tests where the machine was tested for

three continuous days in two seasons (winter and summer). The aim was to achieve good correlation in results from one season test and validate the methodology with good correlation results in different environmental conditions i.e. in a different season. Both tests successfully validated the FEA environmental thermal model with good correlations typically above 60%. This technique in effect can remarkably reduce the machine downtime by creating the CAD model of the machine in the FEA software and simulate it to create an environmental thermal model that is able to simulate the effect of any set of varying environmental conditions.

This method therefore provides a platform to use FEA modelling as an offline tool to determine not only machine behaviour, but also help with the development of compensation models by determining the location of sensitive nodes/areas. The case study by Mian et al. [8, 9] was therefore used for differentiating between areas sensitive to internal heating and environmental temperature fluctuations.

The remainder of the paper details a method and the developed software for the offline assessment of the FEA data and help determine the temperature-displacement sensitive nodes based on search parameters and their physical locations within the FE model. The information can be used to retrofit sensors for compensation; however there can be practical limitations to their attachment.

3. Nodal data extraction

Abaqus simulation software provides the facility to extract surface and sub-surface nodal data within the FEA model. Since the model has to be meshed for FEA analysis, nodes from the mesh can be used to represent individual points on the structure. Therefore, using this facility, the nodal data was extracted to find nodes of interest. The predicted error is obtained as the difference in displacement between a node on the table and a node on the tool. In this case the dependant parameters are slope and hysteresis.

The slope is simply the magnitude of displacement for any given change in temperature ($^{\circ}\text{C}/\mu\text{m}$). Hysteresis is caused by the time lag involved with typical surface temperature measurement which is related to the distance between the temperature sensor and the true effective temperature which is causing the distortion. A node location with high slope sensitivity will require lower resolution in the measurement of temperature and induce less noise when applied in models, as described later. The lowest hysteresis will represent that area that relates well to thermal displacement and responds in a linear fashion whether the machine is being heated or cooled. The nodal data is extracted from Abaqus and the files are converted and imported into Matlab software. Matlab functions were written to calculate the slope and hysteresis for each node and return the best ones with respect to an axis.

3.1. Matlab program routines

The function imports the nodal data from the FEA software and extracts the error between the tool and workpiece in each direction, and the temperature of all the nodes. Then it calculates the slope ($^{\circ}\text{C}/\mu\text{m}$) using a linear least square fit and hysteresis (μm), using deviation from the straight line, for all nodes. These are compared against a predefined set of ranges to filter out the best nodes. The range may be set based on the resolution of the temperature sensors and required accuracy for compensation. There can be thousands of nodes depending on the mesh density of the machine model. If no nodes are found then the range must be widened. The nodes are filtered for slope and hysteresis separately to maintain flexibility so that different nodes can be used for different jobs, not always both. The final node numbers satisfying both filters are then used to locate their positions in the CAD model of the relevant structure. Fig. 1 shows the function calls where comparison takes place using a specified range, in this case the range for the slope sensitivity is from $0.17\text{ }^{\circ}\text{C}/\mu\text{m}$ (min) to $0.20\text{ }^{\circ}\text{C}/\mu\text{m}$ (max) and $5.44\text{ }\mu\text{m}$ (min) to $8\text{ }\mu\text{m}$ (max) for the hysteresis. The first and second lines filter out node numbers for the slope sensitivity and hysteresis respectively using the range. The third line is then used to match node numbers in both arrays and obtain the matched nodes numbers. Fig. 2 shows the Matlab array editor displaying 8 nodes filtered out from the total of 4113 from the carrier (Fig. 5) structure mesh. The first column shows node number, the second column shows slope sensitivities and the third column shows the hysteresis values. These 8 nodes have shown to have the highest slope sensitivities (Fig. 3) and the lowest hysteresis values and will effectively be used to place permanent temperature sensors for use in error compensation systems. It can also be observed that nodes 738 and 739 possess the highest slope sensitivity among the other filtered nodes and a slightly higher hysteresis values relative to the other filtered nodes, however an agreement can be obtained to prioritize the selection of nodes that were located at the surface for practical installation of temperature sensors. This priority may not be the case if slope sensitivities and hysteresis values are significant at node positions inside the structure.

```

Minimum hysteresis sensitivity      Maximum slope sensitivity
chkSlope=filt_slope(:,2<0.17 | filt_slope(:,2)>0.20);
chkHyst=filt_hyst(:,2<5.44 | filt_hyst(:,2)>8);
chk= bitor(chkSlope, chkHyst);
    
```

Fig. 1. Part of Matlab program code for assigning range

	1	2	3
1	519	0.17104	6.2448
2	737	0.19915	7.9239
3	738	0.201	7.8653
4	739	0.20224	7.9583
5	903	0.1713	5.9581
6	2513	0.17765	7.9543
7	2689	0.17452	7.7237
8	2705	0.17246	6.5713

Fig. 2. Filtered nodes

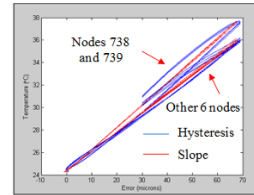


Fig. 3. Slope and hysteresis plot

4. Internal heating test – Carrier sensitivity against the Y axis and Z axis displacement

Since the carrier holds the spindle in place, it is the most affected structure as the heat from the spindle flows directly into it. Therefore, this structure was analysed to locate the temperature-displacement sensitive nodes for internal heating. Fig. 4 shows the visual representation of the simulated deformation of the machine.

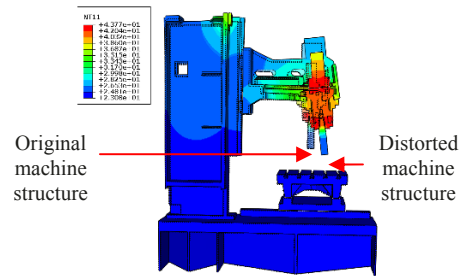


Fig. 4. Simulated visual representation of deformation of the machine due to internal heating

Fig. 5 shows the best surface nodes found using the Matlab search routine. Other visible nodes are inside the structure.

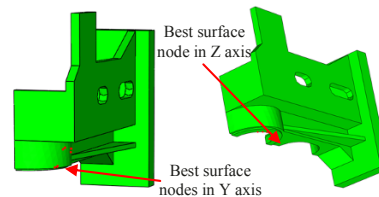


Fig. 5. Nodes sensitive to spindle heating on the carrier

5. Validations

Using the similar approach shown in section 3.1, the best identified surface node (Fig. 6) was checked which give the sensitivity of $0.20^{\circ}\text{C} / \mu\text{m}$ and hysteresis of $7\mu\text{m}$. This linear fit gives a simple model for the Y axis of $5\Delta t_{\text{int}} - 106.5$. This was applied to measured temperature data from a sensor fitted to the machine surface close to the identified node position, with correlation to measured displacement of 84% as shown in Fig.7.

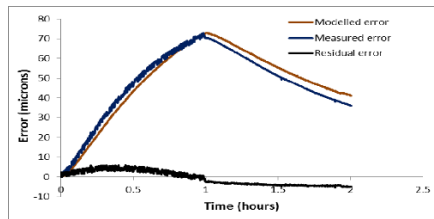


Fig. 6. Validation of the FEA model against measured error due to internal heating

5.1. Environmental sensitive nodes inside the full machine structure

Using the similar procedure the nodes sensitive to the varying environmental conditions, including different seasons, were found in the machine structure. During this preliminary work, each structure was analysed individually for efficiency to locate sensitive nodes with the higher slope and lowest hysteresis approach. Further to consider the full machine structure as one component to locate the set of sensitive nodes. Fig. 7 shows the full machine FEA model with highlighted environmental sensitive nodes individually located on components.

6. Conclusions

It has been observed that the simulation of thermal behaviour of complex machine structures using FEA can provide a solid platform for offline assessment of the machine error and model identification. FEA results from previously conducted case studies were used to locate nodes in the structural elements of a 3 axis VMC that were sensitive to temperature change and movement of the machine structure in Y and Z axes. Matlab functions were used to manipulate the extracted data from the FEA software, calculate the hysteresis and slope for any given node and filter out the best node locations by using a range of highest slope sensitivity and lowest hysteresis value. The location of the filtered nodes were analysed using the Abaqus GUI. The priority is given to surface nodes rather than the internal nodes for practical temperature sensor installation on the machine. The validation result showed the predicted sensitive nodal location correlated to better than 84%. By determining the best linear relationships, simple models are available

and compatible with the common thermal compensation methods available in most modern NC controllers.

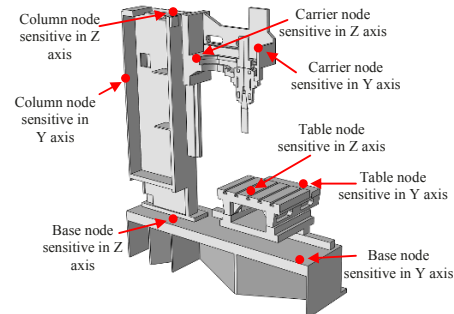


Fig. 7. Environmental sensitive nodes within the full machine

Acknowledgements: The authors gratefully acknowledge the UK's Engineering and Physical Sciences Research Council (EPSRC) funding of the Centre for Advanced Metrology under its innovative manufacturing program.

References

- [1] Bryan, J., International Status of Thermal Error Research (1990). CIRP Annals - Manufacturing Technology, 1990. 39(2): p. 645-656.
- [2] Chen, J.S. and G. Chiou, Quick testing and modeling of thermally-induced errors of CNC machine tools. International Journal of Machine Tools and Manufacture, 1995. 35(7): p. 1063-1074.
- [3] Tseng, P.C., A real-time thermal inaccuracy compensation method on a machining centre. International Journal of Advanced Manufacturing Technology, 1997. 13(3): p. 182-190.
- [4] Yang, S., J. Yuan, and J. Ni, The improvement of thermal error modeling and compensation on machine tools by CMAC neural network. International Journal of Machine Tools and Manufacture, 1996. 36(4): p. 527-537.
- [5] J Yang, J.G., et al., Testing, variable selecting and modeling of thermal errors on an INDEX-G200 turning center. International Journal of Advanced Manufacturing Technology, 2005. 26(7-8): p. 814-818.
- [6] Kang, Y., et al., Estimation of thermal deformation in machine tools using the hybrid autoregressive moving-average - Neural network model. Proceedings of the Institution of Mechanical Engineers, Part B: Journal of Engineering Manufacture, 2006. 220(8): p. 1317-1323
- [7] Debra A, Krulewich., Temperature integration model and measurement point selection for thermally induced machine tool errors. Mechatronics, 1998. 8(4): p. 395-412.
- [8] Mian, N.S., et al., Efficient thermal error prediction in a machine tool using finite element analysis. Measurement Science and Technology, 2011. 22(8): p. 085107.
- [9] Mian, N, Fletcher, S, Longstaff, A.P., Myers, A and Pislaru, C, Efficient offline thermal error modelling strategy for accurate thermal behaviour assessment of the machine tool. In: Proceedings of Computing and Engineering Annual Researchers' Conference 2009: CEARC'09. University of Huddersfield, Huddersfield, pp. 26-32. ISBN 9781862180857.
- [10] ABAQUS/CAE: Hibbit, Karlsson and Sorensen, Inc., Pawtucket, RI 02860-4847, USA.

Development of an Abbé Error compensator for NC machine tools

K. C. Fan, T. H. Wang, C. H. Wang and H. M. Chen

Department of Mechanical Engineering, National Taiwan University, Taiwan, ROC

Abstract. Abbé error is the inherent systematic error in all numerically controlled (NC) machine tools due to the fact that the scale measuring axis is not in line with the cutting axis. Any angular error of the moving stage will result in the position offset from the commanded cutting point. In this report, a new concept of multi-sensor feedback system of the NC controller is presented. A miniature three-axis angular sensor is embedded in each axis to real-time detect angular errors of the moving stage. An error compensator is developed to calculate induced volumetric errors and fed back to the NC controller. This feedback error compensation system automatically corrects the Abbé error of the machine tool. Experiments show that the volumetric accuracy can be improved significantly by employing the proposed Abbe error compensator.

Keywords: machine tools, Abbé error, multi-sensor feedback, volumetric error compensation.

1. Introduction

Abbé error is the inherent systematic error in all numerically controlled (NC) machine tools. the Abbé principle is regarded as the first principle in the design of precision positioning stages, machine tools, and measuring instruments [1]. It defines that the measuring apparatus is to be arranged in such a way that the distance to be measured is a straight-line extension of the graduation used as a scale. Bryan further made a generalized interpretation with that if the Abbé principle is not possible in the system design, either the slideway that transfer the displacement must be free of angular motion or the angular motion data must be obtained to compensate the Abbé error by software [2, 3].

Nowadays, most commercial machine tools and CMMs still cannot comply with Abbé principle because the scale axis is always parallel to the moving axis. A very popular way to improve the accuracy is to store the positioning or volumetric errors through prior measurement or calibration process and then compensate for the error budget with software, which is called the feed-forward compensation [4, 5]. It, however, can only compensate for the mean systematic errors. The angular errors are subject to the time-varied temperature changes. It is known that if the Abbé principle is not possible in the system design, one effective method is to obtain the

real time angular data and compensate for the volumetric error in real-time [6].

Techniques of non-contact angle measurement find applications in many fields. Autocollimators are commonly used optical tools for straightness calibration [7]. Some multi-degree-of-freedom (MDOF) measurement systems have been developed for measuring angular and straightness errors of precision machines but did not feed back to the controller for real-time compensation [8-10]. Laser interferometer, with its superiority in accuracy and resolution, also has been applied for angle measurement [11, 12]. By counting interference fringes the tiny displacement of objective point can be detected and converted into angle value. The resolution can be improved by techniques of phase subdivision to very fine [13]. The author's group has developed a miniature interferometer system for holographic gratings with good performance in measuring uncertainty and signal quality [14].

This paper presents a new approach for real-time Abbé error compensation on the machine tools by hardware. A low-cost three-angle sensor is developed that can embed in each axis of the machine tool. With an appropriate interface connection with the NC controller, this system can successfully compensate for the Abbé error during machine running condition. Experimental results show that the positioning errors within the working volume can be significantly reduced.

2. Abbé error in machine tool

Current NC controller in the machine tool feeds back the scale reading position, which is offset from the real commanded position, as shown in Fig. 1. The straightness error of the slideway will cause angular motion (θ) of the moving table yielding inevitable positioning error (δ) at the cutting point, which is offset from the scale reading position by L .

$$\delta = L \tan(\theta) \quad (1)$$

From the 3D point of view, the moving table has three angular errors, namely pitch, yaw, and roll. Any of these angles will induce positioning errors at the cutting points in three dimensions, as shown in Fig. 2. The corresponding errors can be expressed by the following equation.

$$\begin{bmatrix} \delta_X \\ \delta_Y \\ \delta_Z \end{bmatrix} = \begin{bmatrix} -\theta_Z \cdot L_Y + \theta_Y \cdot L_Z \\ \theta_Z \cdot L_X - \theta_X \cdot L_Z \\ -\theta_Y \cdot L_X + \theta_X \cdot L_Y \end{bmatrix} \quad (2)$$

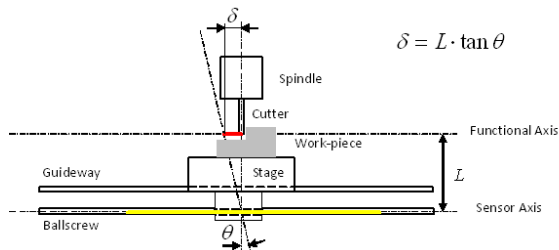


Fig. 1. Abbé error in 1D stage

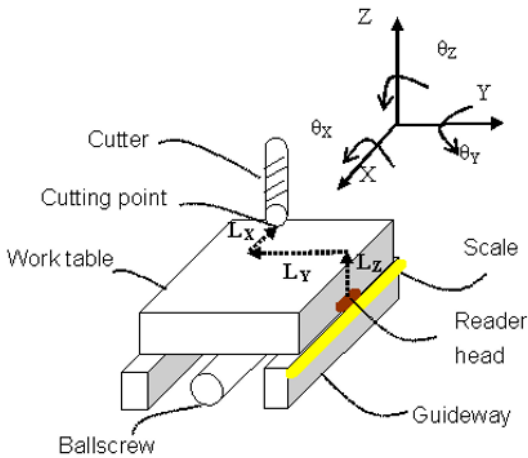


Fig. 2. Abbé error in the 3D space of a linear stage

It is known that to eliminate δ by letting L or θ zero is impossible. The only way is to compensate for the positioning errors by sensing both L and θ and correct the cutting position through the controller. The design of low cost three-angle sensor is necessary.

3. Principle of miniature angular interferometer

The optical structure of the proposed system is shown in Fig. 3. The principle is based on the classic model of Michelson interferometer. The approximately linear polarized beam from the laser diode is split by the polarization beam splitter PBS1. The P-polarized beam

passes through and the S-polarized beam is reflected to the left. With careful rotation of the PBS1 these two beams will have equal intensity. Then, the reflective mirrors M1, M2 and M3 guide these two beams to the object mirror in parallel and equal path distance. When the object mirror has an angle displacement, the change of the optical path difference will cause interference of two returned beams after joining together, which can be converted into corresponding angle value. After passing through the quarter waveplate Q1 twice, the left-arm beam will be converted into P-polarized beam and pass through PBS1. The right-arm beam has the similar feature. This design is to avoid the beam returning back to the laser diode. After passing through Q3 the left-arm beam and right-arm beam will be converted into right-circularly and left-circularly polarized beams, respectively. The NPBS divides both beams into two split beams of equal intensity. These four beams will be separated by 0–90–180–270 degrees by PBS2 and PBS3 (set fast axis to 45 degrees) and interfere with each other. Four photo detectors (PD) will convert the beam intensity to corresponding current. A proper sinusoidal signal processing circuit can reach 0.1 arc-sec resolution. Fig. 4 is the compact size of this developed yaw angle sensor.

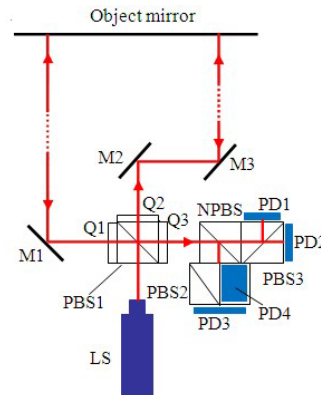


Fig. 3. Optical configuration of angle interferometer

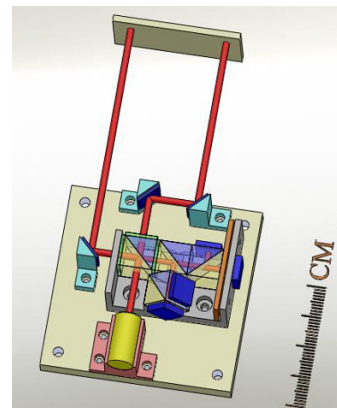


Fig. 4. Design drawing of yaw sensor

4. The Three-angle Sensor

A miniature three-angle sensor has been developed for this purpose, as shown the schematic diagram in Fig. 5. One laser diode splits the beam into two angle interferometer modules set in orthogonal directions, one for the yaw and another for the pitch measurements. The second laser diode also splits the beams to two parallel paths and each one is reflected by a corner cube reflector (CCR) and collected by a quadrant detector. The relative up and down straightness motions of two CCRs reflect the roll angle motion of the stage. Fig. 6 shows the physical size (about 160 mmx 130 mm) of the developed three-angle sensor on one axis of the machine tool. After calibration, the pitch and yaw sensors can reach ± 0.3 sec accuracy for the range of ± 100 sec, and for roll angle it is ± 1 sec accuracy for the range of ± 150 sec. These performances are good enough for machine tool use.

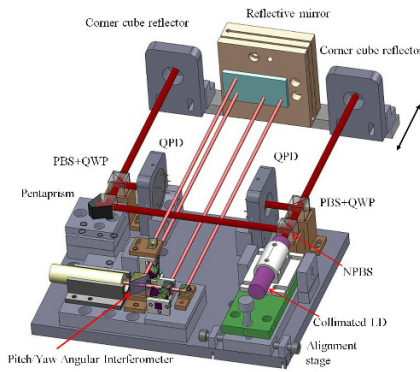


Fig. 5. The integrated structure of a three-angle sensor

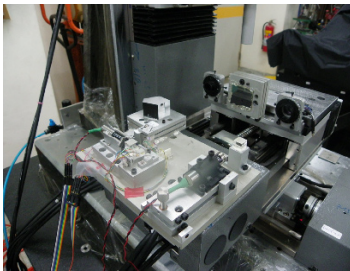


Fig. 6. Photo of a three-angle sensor on the machine tool

5. Experiments

Fig. 7 shows the schematic diagram of mounting the three-angle sensor module on each axis of the machine tool and the integration with the PC-based NC controller. A microprocessor that processes the angle signals and calculates Eq. (2) is called the Abbé error compensator, which can dynamically acquire the current three coordinate positions from the NC controller and, after processing, send the compensated command into the

controller. By this way, the cutting point can be automatically adjusted in real-time with the amount of Abbé errors in space.

A test trial has been carried out on a small NC machine tool. The experimental setup is shown in Fig. 7 for the X-axis motion. A laser interferometer of HP5529 was mounted at different Z heights of the spindle head as a calibration reference. Same procedure can also be conducted for the Y-motion. Figures 8 and 9 show the comparison of positioning errors with and without the Abbé error compensation in X- and Y-axis respectively. The kinematic error of the table can be regarded as a rigid body motion. It is clearly seen that the positioning errors can be significantly reduced when the Abbé error compensation scheme is activated at any position.

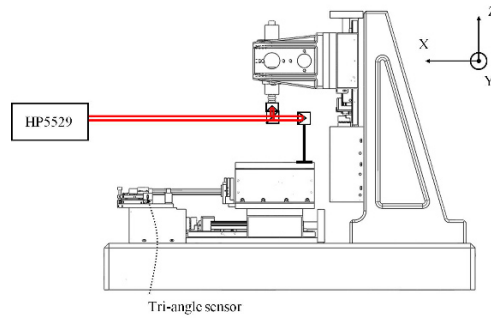


Fig. 7. Experimental setup for positioning test

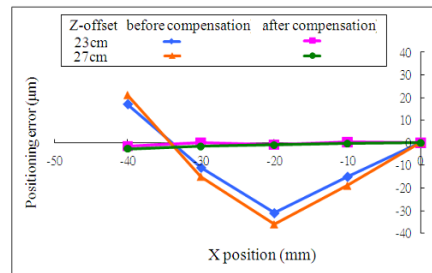


Fig. 8. Experimental results of X-positioning error calibration.

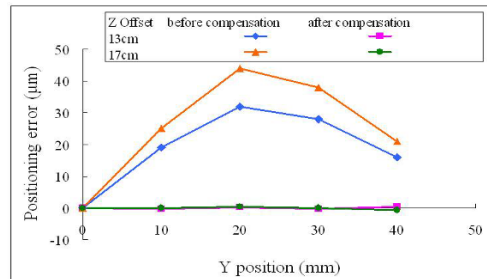


Fig. 9. Results of Y-positioning error calibration

6. Conclusions

In this paper, a developed low cost miniature three-angle sensor module is presented. It is able to embed in the machine tool structure and compensate for the positioning errors within the working zone. The developed Abbé error compensator can be equipped to any machine tool for real-time Abbé error compensation. Experimental results show the effectiveness of this system. Since this is a real-time feedback error compensation system, it can realize the goal of time-variant volumetric error compensation on any NC machine tool.

References

- [1] Abbé E, (1890) Meßapparate für physiker. Zeitschrift für Instrumentenkunde 10: 446–448
- [2] Bryan JB, (1979) The Abbé principle revisit: An updated interpretation. Precision Engineering 1: 129–132
- [3] Wright DA and Bryan JB, (1979) Letters. Precision Engineering 2: p2.
- [4] Ni J and Wu SM, (1993) An on-line measurement technique for machine volumetric error compensation. ASME J of Engineering for Industry 115: 85–92.
- [5] Okafor AC, Ertekin YM, (2000) Derivation of machine tool error models and error compensation procedure for three axes vertical machining center using rigid body kinematics. International J of machine Tools & Manufacture 40: 1199–1213.
- [6] Huang PH and Ni J, (1995) On-line error compensation of coordinate measuring machines. International J of Machine Tools 35: 725–738.
- [7] Yoder PR, Schlesinger JE, and Chickvary JL, (1975) Active annular beam laser autocollimator system. Applied Optics 14: 1890–1895.
- [8] Fan KC, Chen MJ and Huang WM, (1998) A six-degree-of-freedom measurement system for the motion accuracy of linear stages. Int. J. of Machine Tools & Manufacture 38: 155–164.
- [9] Liu CH, Hsu CC, Jywe WY and Hsu TH, (2005) Development of a laser-based high-precision six-degrees-of-freedom motion errors measuring system for linear stage. Review of Scientific Instruments 76: 055110-1–055110-6.
- [10] Gao W, Arai Y, Shibuya A, Kiyono S and Park CH, (2006) Measurement of multi-degree-of-freedom error motions of a precision linear air-bearing stage. Precision Engineering 30: 96–103.
- [11] Jablonski ER, (1986) Interferometric measurement of angles. Measurement 4 (4): 148-153.
- [12] Ikram M and Hussain G, (1999) Michelson interferometer for precision angle measurement. Applied Optics 38: 113–120.
- [13] Brich KP, (1990) Optical fringe subdivision with nanometric accuracy. Precision Engineering 12: 195-198.
- [14] Cheng F and Fan KC (2011) A linear diffraction grating interferometer with high alignment tolerance and high accuracy. Applied Optics 50: 4550-4556.

A novel haptic model and environment for maxillofacial surgical operation planning and manipulation

X-T Yan¹, E Hernandez², V Arnez², E Govea³, T Lim⁴, Y Li¹, J Corney¹ and V Villela²

¹Design, Manufacture & Engineering Management, University of Strathclyde, Glasgow, UK

²Facultad de Ingeniería, Universidad Nacional Autónoma de México, D.F. México

³Centro de Investigación y Estudios de Posgrado, Facultad de Ingeniería, Universidad Autónoma de San Luis Potosí, S.L.P. México

⁴Innovative Manufacturing Research Centre, Heriot-Watt University, Edinburgh, UK

arnezvictor@comunidad.unam.mx²

Abstract. This paper presents a practical method and a new haptic model to support manipulations of bones and their segments during the planning of a surgical operation in a virtual environment using a haptic interface. To perform an effective dental surgery it is important to have all the operation related information of the patient available beforehand in order to plan the operation and avoid any complications. A haptic interface with a virtual and accurate patient model to support the planning of bone cuts is therefore critical, useful and necessary for the surgeons. The system proposed uses DICOM images taken from a digital tomography scanner and creates a mesh model of the filtered skull, from which the jaw bone can be isolated for further use. A novel solution for cutting the bones has been developed and it uses the haptic tool to determine and define the bone-cutting plane in the bone, and this new approach creates three new meshes of the original model. Using this approach the computational power is optimized and a real time feedback can be achieved during all bone manipulations. During the movement of the mesh cutting, a novel friction profile is predefined in the haptical system to simulate the force feedback feel of different densities in the bone.

Keywords: Haptic surgical planning, mesh model, bone cutting, DICOM images, process planning, friction model.

1. Introduction

During the last decade there have been several research efforts [1-4] to achieve an interface with which the user could do practices in medicine, without the need to use a human body or animal, all immersed in a virtual environment. In order to enhance this work a haptic property is added, having said that, many researchers have been driven to develop a system that is realistic in both feeling and visual [5-6].

The increasing research interests into tactile displays and haptic feedback systems to augment virtual reality in the last five years have led to trial haptic devices that aid the training of hand-based skills in applications such as

medical training. There are commercially available devices such as the PHANTOM by Sensable Technologies [7] and the Cyberglove by Immersion Inc. [8]. Research has already been conducted into simulating jaws, body parts and so on using such devices. However, these devices are designed to give haptic feedback for relatively lower resolution and large surface areas to give the impression of interacting with large volumes, and cannot provide the correct force feedback. The devices were therefore found to be unsuitable for haptic feedback. In addition, the extremely high cost of these devices makes them inaccessible to mass medical training.

This paper describes findings of research work undertaken in collaboration among authors from several institutions on the application of haptic technology and development of a haptic model for maxillofacial operation planning and training. This haptic environment has been used in conjunction with medical images obtained from computerized tomography scanners, looking to train medical doctors and in some cases to plan surgical operations.

The solutions in physics are implemented in an environment that generates a friction and stiffness on the body, both forces have been studied and reported several times, but the solutions in visual environments are mainly going in two ways, one using polygonal meshes and the other using voxels. Both types of solutions have their own difficulties when interacting with the physics solutions. When using meshes, the computational power tends to be exhaustive when detecting collisions and doing a cutting function, but the resolution can be good enough for medical purposes. In more recent work, the use of voxels is becoming more present since they need less computational power to handle cutting functions and detecting collisions, but in the counter part they are not very accurate for some particular applications.

The need to develop a method that achieves a precise cutting function with a computational power enough to maintain a haptic rendering is paramount at this stage of the study. It is because of this that the objective of the present paper is to design and develop a haptic interface that uses few computational resources, allowing having a real-time feedback and a good resolution when cutting the model.

2. Image capture of a subject's head

2.1. DICOM images processing

CT scans are commonly used to scan a patient and capture the tissues, bone void etc in many slices of images. A CT scan model is provided for this research to develop a haptic model for geometry representation of a patient head. At this first stage the images captured by the CT are counted, and these images are in an unrecognizable format for the computer without the specific software. They consist in a series of files inside a folder where each file contains the information that describes the material density of a transversal section of the patient's body: in other words, is the radiography taken of a specific plane of the patient, in this manner, by joining all the images together a 3D image of the body can be reconstructed.

To achieve this image compilation and the representation as a volumetric body, the VTK (Visualization ToolKit) libraries were used in this research. These libraries have functions that allow an easy management of the images and the graphic resources of the computer, and they are built on top of the open software OpenGL, which is the standard in graphics management for various operating systems such as Microsoft Windows.

To compile a series of images stored in the folder, it is essential to develop an appropriate algorithm to construct the three-dimensional model of the patient. The algorithm of the program to read the DICOM images (images taken from the CT) is as follows:

- Create a VTK variable to read DICOM files. Load the address where the images are allocated in the computer memory.
- Make sure that the model is in three dimensions.
- Apply a reduction factor.
- Create a variable to allocate the volume information.
- Add the properties of colour and volume opacity.
- Apply filters to the variable that contains the information of the DICOM images. These filters are: contour filter, triangle filter to generate the mesh, decimation, cleaning the mesh of non-connected points.
- Generate a STL file.

- Draw the volume on screen to visualize the result.
- End program.

Codifying the above algorithm it is possible for the program to create a window to visualize the DICOM images and a file with in STL format. The generated image represents a skull for this example, and the program adds some properties to make it look like bone shown in Fig. 1.



Fig. 1. DICOM images representation.

2.2. Partition the jaw part from the head model

As the research is to focus on the support of surgical maxillofacial operations, it is more efficient to extract the jaw model only in order to minimise the computational burden for haptic modelling. For this phase no filter generated by computational algorithms is needed, the reason is that an image processing based on the human anatomy is required, and to do so the human knowledge is needed. Because of this, the software MeshLab is used, which in essence reads the STL file and shows it on the screen. In addition, it gives the freedom to edit the mesh file manually: that is, it supports the manipulation of the geometry by selecting the points and faces with the mouse. This provides freedom for more accurate and smooth operations of the model if necessary.

Since the jaw is required to be isolated from the skull (Fig. 2), a computational tool could be used to save time and effort in some circumstances. This tool is a filter implemented in VTK that allows to delete from the mesh all of the points and faces that have no connection with the biggest continuous volume in the file. This tool can be executed as many times as needed during this phase.

The algorithm to apply this filter is as follows:

- Create a VTK variable to read the STL file. To load the address of the file in the variable.
- Apply the connexion filter to the previous variable.
- Create a STL file with the resulting information after the filter.
- End program.

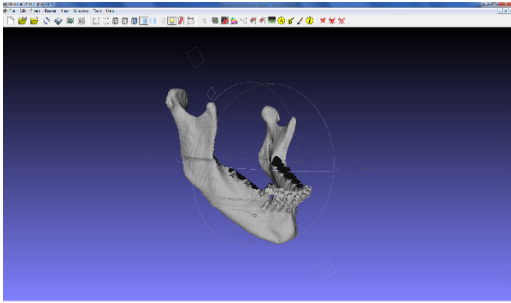


Fig. 2. Jaw obtained.

For the purpose of demonstration of concept and for future tests, a portion (Fig. 3) of the previous mesh is selected and used, and it is the right side of the bone.

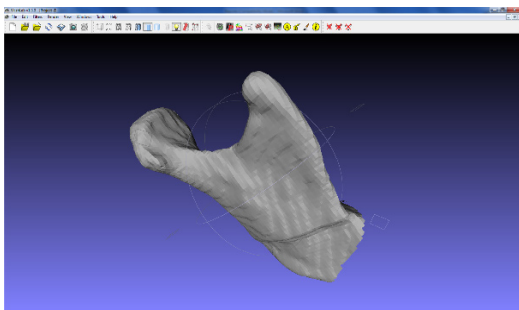


Fig. 3. Portion of the jaw.

3. Haptic model

3.1. Preparing the cut

This third phase is the main objective of the work in this project, because it involves adding the cutting function to a haptic interface. All the load of the work goes directly over C++ using VTK libraries.

The algorithm for the cut is as follows:

- Create a VTK variable to read STL files. To load the address of the STL file to use.
- Call a cutting function giving the Cartesian coordinates of the position where the cut is required.
- Inside the cutting function, use a VTK function to extract geometries from the VTK variable that contains the mesh information.
- Create a widget using the data received in the cutting function as arguments, and using a thickness proportional to the surgical tool.
- Filter the result to eliminate all the points and faces that have no continuity with the larger volume.
- Obtain the resulting mesh after retrieving the specified geometry.

- Apply the filter to remove just the points that have no connexion within the mesh.
- Display the result on screen.
- End program.

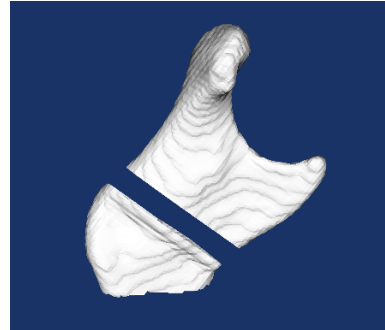


Fig. 4. Cut jawbone by the middle with a box with thickness of 5 graphic units, the faces of the box are coplanar with the planes xy , xz and yz .

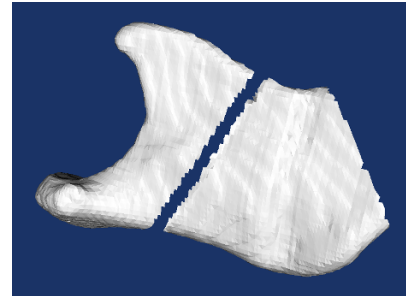


Fig. 5. Cut jawbone with thickness of 4 graphic units, the faces of the box are oriented 30 degrees from the planes xy , xz and yz .

3.2. Haptic interface

To create the interface a tool was added to the omniscursor. The reason is to obtain a point from which the cutting function will be applied and also calculate an orientation and depth of the cut. Having all this information set, the function can create a friction profile to interact with the piece of the bone that has been cut and give the feeling of being removing material from the original mesh.

Once the omniscursor from the haptic device is in place and the user clicks the primary button of the haptic tool, two main things happened after, the position and orientation of the tool is obtained and the farthest point of the mesh in the orientation of the tool is calculated. The next thing to operate is that the mesh is cut graphically and the movement of the tool is then restricted only to push the cut piece inside the mesh, as if the user would be actually cutting it. In order to give a more realistic feeling, a novel friction profile is created to the movement of the tool.

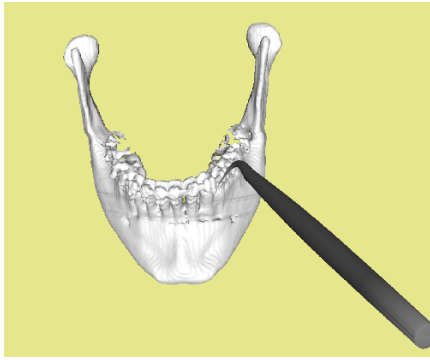


Fig. 6. Haptic interface.

3.3. Friction and stiffness profile

In this section the physical characteristics are given to the cutting body, such as the dynamic friction and the stiffness, a surgeon can adjust both in order to make the feel of operation more realistic.

The work with friction (Fig. 7) needs to define a maximum and a minimum of this variable, the first represents the bone and the second the bone marrow. The importance of these two friction values is that they are not the friction felt when moving the omniscursor in the surface of the mesh, but when the omniscursor is moving inside the mesh, so the feeling can be interpreted as cutting the bone.

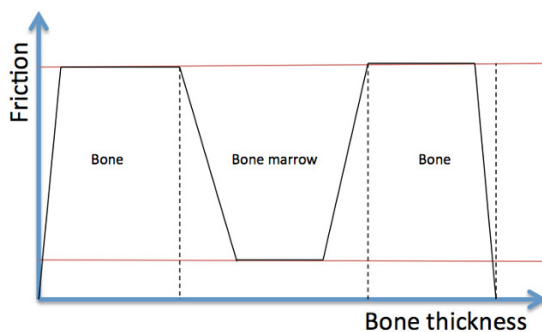


Fig. 7. Friction profile.

What the user will see is that the mesh was cut at the moment the user pushes the button and then the user is holding the cut piece and pushes it inside the bone. This makes the user feel like cutting. Once the movement is complete and the omniscursor is on the other side of the bone, the cut piece disappears and the user is ready to cut the bone in other part.

4. Conclusions

A new method to achieve real-time force feedback with a cutting function of polygonal meshes in a virtual jaw

model environment was developed. This solution has enabled the real feeling of bone friction and stiffness, even during the cut function. It can maintain stability in the haptic device since the movement is restricted and no collision detection is required. The main significance and implication of this research are obtaining a precise cut in the polygonal mesh, which is more precise than a voxel model and in real time and less requirement on computational resources, which has been the main problem when using polygonal meshes. Future work consists of generating different shapes of cut, with different tools, to create different suitable resistance to emulate the real time cutting experience. It is also planned to try the system with surgeons and evaluate the degrees of real feel and to create a better cutting algorithm in order to obtain a sharper mesh after applying the function.

Acknowledgements: We would like to thank CONACyT in Mexico for the support given in the form of scholarship during the work of this project. Another thanks for Universidad Nacional Autónoma de México in Mexico City, Mexico, the Universidad Autónoma de San Luis Potosí in S.L.P., Mexico and the University of Strathclyde in Glasgow, UK.

References

- [1] Xia J.J., Phillips C.V., Gateno J., Teichgraber J.F., Christensen A.M., Gliddon M.J., Lemoine J.J., Liebschner M.A.K., Cost-Effectiveness Analysis for Computer-Aided Surgical Simulation in Complex Cranio-Maxillofacial Surgery, *Journal of Oral and Maxillofacial Surgery*, 64(12):1780-1784, 2006
- [2] G. Moy, U. Singh, E. Tan, and R. S. Fearing, "Human psychophysics for teleaction system design," *Haptics-e, The Electronic Journal of Haptics Research*, vol. 1, 2000.
- [3] K. McGovern, and R. Johnston, "The Role of Computer-Based Simulation for Training Surgeons," *Studies in Health Technology and Informatics: Medicine Meets Virtual Reality: Health Care in the Information Age*, Vol. 29, pp. 342-345, 1996.
- [4] A. Crossan, S. A. Brewster, S. Reid, and D. Mellor, "Multi-Session VR Medical Training – The HOPS Simulator," *British Computer Society Human Computer Interaction*, London, UK, pp. 213-226, 2002.
- [5] R. L. Williams, J. N. Howell, M. Srivastava, and R. R. Conaster Jr, "The Virtual Haptic Back Project," *IMAGE 2003 Conference*, Scottsdale, Arizona, USA, 2003.
- [6] G. Burdea, G. Patounakis, and V. Popescu, "Virtual Reality-Based Training for the Diagnosis of Prostate Cancer," *IEEE Transactions on Biomedical Engineering*, pp. 1253-1260, 1999.
- [7] <http://www.sensable.com>
- [8] <http://www.immersion.com>

“LCA to go” – Environmental assessment of machine tools according to requirements of Small and Medium-sized Enterprises (SMEs) – development of the methodological concept

R. Pamminer, S. Gottschall and W. Wimmer
Institute for Engineering Design, Vienna University of Technology, Austria

Abstract. The goal of the “LCA to go” project is spreading the use of LCA across European SMEs. For the sector of machine tools a webtool will be developed to help SMEs with conducting environmental assessment. First the SMEs requirements regarding environmental assessment were gathered in a survey. Second LCA case studies and third standards and legislation were studied. Out of these three sources a simplified environmental assessment methodology is developed. This resulted in a two-step approach including the life cycle phase raw materials and use phase of the machine tool. In the first step of the methodology the Cumulative Energy Demand have to be calculated to analyse the environmental hot spots. Depending on the hot spots a detailed environmental assessment using the CED or an Energy Efficiency Index is proposed in the second step. The methodology should be kept simple but lead to useful data for environmental communication. Next steps in the project are the detailed specification of the methodology, the data collection and the tool development.

Keywords: Environmental assessment methodology, machine tools, SMEs

1. Introduction

Environment is one of the leading concerns of our industrialized life. The increasing interest in environmental impacts of products over the whole life cycle is reflected by the numerous standards and activities. Large sized companies have enough budget and workforce to cope with these environmental necessities, but what about SMEs? The objective of the project “LCA to go” is to develop open source webtools for SMEs to perform a sector specific life cycle based environmental assessment. It provides tailor-made solutions to integrate simplified life cycle approaches into daily business processes. Industry machines and more specifically machine tool are in focus of the “LCA to go” project next to other sectors.

2. Approach

This paper shows the development of the methodology concept for the environmental assessment of machine tools. To name an appropriate assessment method (LCA, Carbon Footprint, Energy Efficiency Index etc.) a SMEs needs assessment in form of a survey, a research for current case studies of environmental assessments of machine tools and an analysis of current and future legislation and standards have been conducted (Fig. 1).

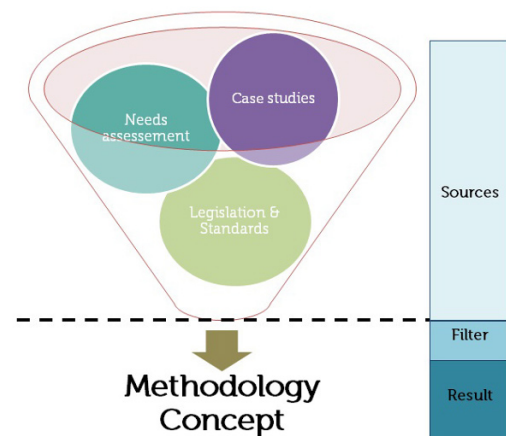


Fig. 1. Development of methodology concept [1]

2.1. Needs assessment

A survey, where 22 SMEs specialized in machine tool manufacturing responded, helped to define the needs of the European SMEs. It can be recognized that environmental issues are already anchored in SMEs but often just in form of cleaner production and theoretical knowledge around environmental assessment methods.

Only 2 companies have practiced LCA once and just 36% of respondents know that machine tool are use-intensive products (because of energy consumption). 23% think that disposal is the most problematic life cycle (Fig. 2).

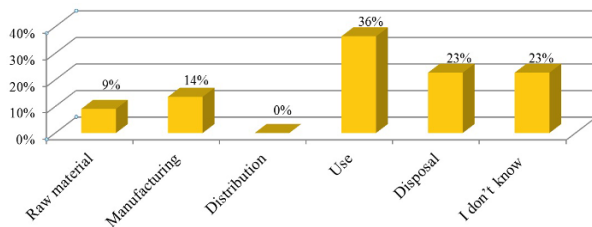


Fig. 2. Survey answers to the question “What is the most problematic life cycle phase of a machine tool?” [1]

Nevertheless the SMEs pointed out that the software tool should focus on energy aspects and it should support in fulfilling legal requirements. As environmental communication instrument a voluntary environmental label focusing on energy efficiency is of most interest. Additionally the tool should help improving product quality, product environmental performance should support in reducing manufacturing costs and helps to be prepared for future requests according to customers' demands. It should be possible to assess innovative products, without complete life cycle data sets.

2.2. Case studies

Case studies about environmental assessment of machine tools give the scientific perspective via providing environmental profiles where the most environmental aspects can be derived.

For conducting an LCA of machine tools different methods (CML, Ecoindicator 99, Cumulative Energy Demand) have been used in the case studies. Machine tools have usually a high weight (> 5 tons) and average lifetime of about 10 years running on a 2-3 shift basis. The result of the environmental assessment pointed out that the energy consumption during use phase causes 55-90% of the total environmental impact. Fig. 3 shows the environmental profile for an injection moulding machine. Additionally the energy consumption in the use phase is broken down into its main consumer, where the tempering unit is of main importance consuming nearly 50% of the total energy consumption.

Further the case studies showed that only for least intensive used machines e.g. one shift operation of a press brake, the raw material use has a relevant environmental impact with 40% of the total. This indicates that the environmental impact of a machine tool is quite sensitive according to the use scenario.

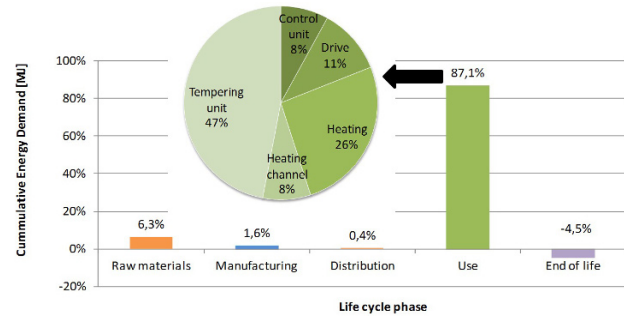


Fig. 3. Environmental Profile of an injection moulding machine [2]

2.3. Legislation and Standards

To ensure a high application rate of the developed web tool, the methodology should be in line with the actual and future legislation and standards.

Machine tools are already in focus of different environmental driven legislative initiatives. The European Commission has started a Product Group Study related to the Ecodesign Directive [3] with the aim to identify and recommend ways on how to improve the environmental performance of machine tools. This pressure from the EC resulted in two further initiatives driven by the industry. The ISO 14955 [4] and the Self-Regulation Initiative [5] concentrate on the environmental assessment of machine tool. The SRI and the ISO focus on the evaluation of energy efficiency of machine tools, where according to the functions of a component their energy consumption is allocated and the most relevant machine components can be identified. Further the German Society on Numeric Control (NCG) [6] proposed a method to measure the energy usage to calculate an Energy Efficiency Index (EEI).

All mentioned initiatives and standards are focusing on the energy consumption during the use phase of a machine tool. Additionally, also Product Category Rules for preparation of an Environmental Product Declaration are under development, where the whole life cycle is considered [7].

2.4. Methodological concept

According to some leading questions the key aspects of the methodological concept is identified (see Table 1). These questions are answered on the basis of the three defined sources needs assessment, the case studies and the legislation.

For machine tools the most relevant environmental aspect is the energy consumption during use as it is of major importance according to all three sources. The energy consumption represents up to 90% of the total environmental impact of a machine tool, already first attempts in legislation are seen and also the companies get more and more aware of this issue.

Table 1. Main questions leading to methodological key aspects (excerpt) [1]

Main questions	Sources	Key aspects for methodology
On which environmental aspect(s) the assessment should focus?	Case studies, Needs assessment,	Energy consumption, materials consumption
What kind of environmental assessment should be provided?	Case studies, Needs assessment	Cumulative Energy Demand (MJ), Energy Efficiency Index (kWh/production unit)
What kind of environmental communication instrument should be used?	Needs assessment, Legislation	Energy savings, EEI, CED

Additionally the raw material use is the second relevant environmental aspect to consider as they are relevant for the companies (needs assessment) and also due to some environmental assessment case studies. The relative environmental impact of the raw materials rises, especially if the machines running just a few hours a week and less energy are used during the whole life of the machine. Materials become also important, when large quantities or rare elements are addressed within machine tools or if the customer’s request a material declaration. Moreover increasing costs of materials or future legislation could bring these aspects more in focus.

Therefore, the environmental assessment method as well as the developed software tool will be limited on the relevant life cycle phase raw materials and use phase. Parameters such as auxiliary materials or energy consumption during manufacturing of the machine tool are excluded as this causes minor environmental impact over the full life cycle of the machine tool. For environmental communication a voluntary environmental label, focusing on energy efficiency, is of most interest. SMEs want to inform their business clients about energy savings of machines compared to reference products.

To fulfil these key requirements a two-step assessment is proposed. In the first step a hot spot assessment with applying the Cumulative Energy Demand (CED) will be conducted. Just the impacts of indicators for energy and for materials are in focus of the assessment. In the second step a detailed assessment will be conducted, either an EEI or a more specific CED will be calculated.

2.4.1. First step: Hot spot assessment with CED

The goal in the first step is to find the environmental hot spot of the machine tool. With only limited data input the dominant environmental life cycle phase can be highlighted. According to these results a detailed assessment can be conducted in the second step.

The CED is an appropriate approach to assess impacts due to energy and material consumption leading to aggregated results in MJ. The results are easy understandable for SMEs. In the material section a rough estimation of the CED will be calculated. Just knowing

the total weight of the machine tool the CED is calculated using a general material data set, including an average material mix. Then the main focus lies in the definition of the use scenario. Therefore the operating hours of the machine tool over the full life time have to be assessed. It has to be declared if the machine is used in 1-shift, 2-shift or 3-shift operation and what is the targeted lifetime. Within one shift different machine modes (operating, stand-by, idle) have to be considered. For all this machine modes the energy consumption has to be measured according to a defined measuring standard. As result the environmental performance just focusing on raw materials and the use phase, calculated in MJ is given. If the CED shows a significant environmental impact of both raw materials (>10% of the total CED) and the use phase than the CED should be used for further environmental considerations – step two. If the CED of the materials represents less than 10% of the total energy the detailed environmental assessment should focus just on the use phase. In this case an Energy Efficiency Index (EEI) will be calculated.

2.4.2. Second step: Detailed assessment with CED or EEI

To get accurate results in the second step the environmental assessment will be conducted in more detail. If the accuracy rises to a certain level e.g. 95% of the environmental impact, the results can be used for environmental communication as well. Additionally the results should help and give advice on how to environmentally improve the machine tool.

In case of significant environmental impact of both the materials and the use phase the CED will be calculated in more detail. Therefore the specific materials have to be declared. For each material a dataset is available. The more materials are declared the higher the accuracy of the results. In the use phase the energy consumption is measured according to the energy measurement standard giving the energy consumption for all main components. This will help at the analysing stage when it comes to product improvement.

In comparison to other environmental assessment methods the advantage of the CED methodology is manageable data and time effort, which was a main

criterion for SMEs using an environmental assessment method. Moreover it delivers easy to understand results, even for users which have low experience in the field of environmental assessment.

If the use phase is dominating an EEI should be calculated instead of the CED. An EEI has the purpose to assess the energy efficiency of products and to show the efficiency performance in comparison to other products. The EEI is also very much favoured as business to business communication from the SMEs, as it provides clear and short information about energy consumption of a machine tool during the use phase. In comparison to other communication instruments like the product carbon footprint (PCF) the EEI methodology is easy to calculate and to understand. Moreover the value of the EEI is the same for a specific product in every country. Considering a PCF (calculated with CO₂-equivalents) the value for one and the same product is different due to the different energy mixes.

In developing an EEI, the challenge is to get comparable results. This has to be secured by defining a suitable energy measurement standard. For example, NCG has proposed a standard where the machine has to run through a 15 min test cycle without producing a work piece. This leads to a method applicable for a broad range of machine tools, but on the other side the productivity and the energy consumption during production are not included. Another approach to define specific test pieces like it is foreseen in the ISO/CD 14955-1 Part 3. This lead also to comparable results but a test piece for each product type is needed.

In Fig. 4 a model on how to display the energy efficiency of a product is shown. The energy efficiency is defined as the relation of the energy consumption to the production unit per hour. Within this model the energy efficiency of a machine tool can be compared with other machine tools and additionally the energy class (A, B, C, etc.) can be defined. For example machines with the Best Available Technology (BAT) represent the energy class B or machines with Best Not Yet Available Technology (BNAT) are defined as class A. This energy classes can then also be used within an Energy Efficiency Label for environmental communication.

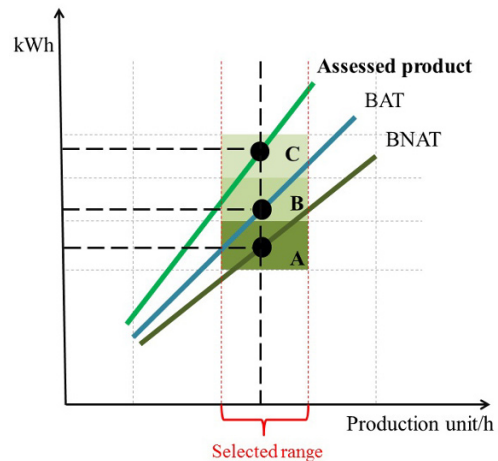


Fig. 4. Model of Energy Efficiency Index

3. Outlook

In the next step a simplified operating method is generated including compiling environmental profiles and developing Product Category Rules (PCR). To define the EEI the challenges will be the definition of the measurement standards and the data collection for reference products (BAT, BNAT). More aspects to clarify are the definition of the use scenarios and the energy measurement standard. Defining the details of the tool and the methodology will be conducted in collaboration with the later users, the SMEs.

References

- [1] Pamminer R, (2012) Deliverable 1.2: Methodology concepts for LCA support of SMEs, EU-FP7 Project, LCA2go Project, GA Nr. 265096
- [2] Pamminer R, Wimmer W, Winkler R (2009) Entwicklung von Kriterien zur Kommunikation der Energieeffizienz von Kunststoff verarbeitenden Maschinen. Berichte aus Energie und Umweltforschung 5/2010
- [3] Schischke K, (2010) Energy-Using Product Group Analysis, Lot 5: Machine tools and related machinery, Executive Summary – Version 2
- [4] ISO/CD 14955-1 (2011) Machine tools - Environmental evaluation of machine tools Part 1: Design methodology for energy-efficient machine tools
- [5] CECIMO (2010) Concept Description for CECIMO's Regulatory Initiative (SRI) for Sector Specific Implementation of the Directive 2005/32/EC (EuP Directive), PE International GmbH
- [6] Kaufeld M, (2011) Energieeffizienz – eine Kennziffer a' la NCG für den Anwender, NC transfer, Nr. 49
- [7] PCR 44214 (2011) Product Category Rules CPC 44214: Machine-tools for drilling, boring or milling metal, open consultation version, 29.09.2011, EPD International System.

Analytical modeling of the machine tool spindle dynamics under operational conditions

O. Özşahin¹, E. Budak², H. N. Özgüven¹

¹Middle East Technical University, Department of Mechanical Engineering, Ankara, Turkey

²Sabanci University, Faculty of Engineering and Natural Sciences, İstanbul, Turkey

Abstract. Chatter is an important problem in machining operations, and can be avoided by utilizing stability diagrams which are generated using frequency response functions (FRF) at the tool tip. In general, tool point FRF is obtained experimentally or analytically for the idle state of the machine. However, during high speed cutting operations, gyroscopic effects and changes of contact stiffness and damping at the interfaces as well as the changes in the bearing properties may lead to variations in the tool point FRF. Thus, stability diagrams obtained using the idle state FRFs may not provide accurate predictions in such cases. Spindle, holder and tool can be modeled analytically; however variations under operational conditions must be included in order to have accurate predictions. In authors previous works Timoshenko beam model was employed and subassembly FRFs were coupled by using receptance coupling method. In this paper, extension of the model to the prediction of operational FRFs is presented. In order to include the rotational effects on the system dynamics, gyroscopic terms are added to the Timoshenko beam model. Variations of the bearing parameters are included by structural modification techniques. Thus, for various spindle speeds, and holder and tool combinations, the tool point FRFs can be predicted and used in stability diagrams.

Keywords: Machine Tool Dynamics, Chatter, Gyroscopic Effects

1. Introduction

In high speed machining operations, stability diagrams can be used to avoid chatter [1-3] and accurate tool point FRFs are needed for determination of the stability diagrams which is usually obtained for the idle state of the machine tool [4-6]. Inconsistent results, on the other hand, are frequently observed between the actual and the predicted stability especially at high spindle speeds which can be attributed to the changes of the dynamic properties of the structures during cutting. With the development of the noncontact measurement devices such as Laser Doppler Vibrometer (LDV), variation of the machining center dynamics during cutting operations has been investigated experimentally and significant deviations have been observed [7-8].

At high speeds gyroscopic moments, centrifugal forces and thermal expansions cause variations in

machine dynamics. In addition to the structural variations due to the rotational effects, bearing properties are also affected by the gyroscopic moments and centrifugal forces [9-11]. In order to analyze these effects Finite Element Modeling (FEM) has been used [12-13].

In this paper, a complete model for a machining center under operational conditions is presented by extending the previously developed analytical spindle-holder-tool assembly dynamics model by the authors [5], including the variations under operational conditions. The spindle, holder and tool subassemblies of the machining center are modeled analytically by using the Timoshenko beam model including gyroscopic effects. The subassembly FRFs are coupled using receptance coupling method with the contact parameters at the spindle – holder and holder – tool interfaces. In addition to the structural dynamics, bearing properties are also added to the system with structural modification techniques. Since bearing properties mainly affect the spindle modes, and these properties vary during cutting, speed dependent bearing properties are adapted to the model. Finally speed dependent tool point FRF, and thus stability diagrams are obtained, and variations of the chatter stability under operational conditions is investigated.

2. Model development

2.1 Component modeling

The Timoshenko beam model was used for modeling of the spindle-holder-tool dynamics by Erturk et al. [6]. In order to include the gyroscopic effects rotary inertia should be included in the beam model. Therefore, Euler-Bernoulli beam model cannot be used for modeling a rotating structure. Furthermore, for low slenderness ratios, shear deformation becomes important at high frequencies. The Rayleigh beam model which includes rotary inertia effects but neglects shear deformation does

not provide accurate results. Therefore, for accurate modeling of the system, the Timoshenko beam model is used.

Equation of motion for the rotating Timoshenko beam can be written as follows:

$$EI_x \frac{\partial^4 u_y}{\partial z^4} + \rho A \frac{\partial^2 u_y}{\partial t^2} - \rho I_y \left(1 + \frac{E}{kG} \right) \frac{\partial^4 u_y}{\partial z^2 \partial t^2} + \frac{\rho^2 I}{kG} \frac{\partial^4 u_y}{\partial t^4} + 2\rho I_y \Omega \left(\frac{\partial^2}{\partial z^2} \left(\frac{\partial u_x}{\partial t} \right) - \frac{\rho}{kG} \frac{\partial^3 u_x}{\partial t^3} \right) = 0 \quad (1)$$

where ρ is the density, A is the cross sectional area, I is the area moment of inertia of the beam cross section about neutral axis, G is the shear modulus, k is the shear coefficient and Ω is the spin speed of the beam.

As seen from equation 1, due to the gyroscopic effects, motions in two orthogonal planes are coupled. Therefore, classical solution methods cannot be applied for the rotational Timoshenko beam equations. However, since the element is axially symmetric, it is known that the mode shapes of the beam in two orthogonal planes will be related to each other by the following relations:

$$U_x(z) = iU_y(z) \quad U_x(z) = -iU_y(z) \quad (2)$$

Modes given by equations 2 correspond to the forward and backward modes in rotor dynamics, respectively. For the harmonic forcing case and axially symmetric geometry, linear displacements in two orthogonal planes can be decoupled and equation for the backward and forward motions in each orthogonal plane can be obtained. Thus, the solution procedure given by Aristizabal [14] can be applied to the Timoshenko beam model with the additional gyroscopic terms, and the mode shapes can be determined for the free-free boundary conditions. Finally, since the rotating Timoshenko beam model is a non-self adjoint system, by using the right and adjoint left eigenvectors, biorthonormality can be applied [15-17] and the receptance functions of the beam element can be obtained as follows:

$$H_{ij}(\omega) = \sum_0^{\infty} \left(\frac{U_{y_r}(x_i) \bar{U}_{y_r}^a(x_j) F(t)}{i\omega - \lambda_r} + \frac{\bar{U}_{y_r}(x_i) U_{y_r}^a(x_j) F(t)}{i\omega - \bar{\lambda}_r} \right) \quad (3)$$

In order to check the accuracy of the proposed method, the analytical predictions are compared with the FEM results. End point FRF of a 1 m long beam with 60 mm diameter is determined using ANSYS and compared with the analytical solution in Fig. 1 which shows very good agreement.

2.2 Receptance coupling

Spindle-holder-tool assembly dynamics can be modeled using the receptance coupling method where the

subassembly components are modeled using the Timoshenko beam model presented in the previous section along with the contact parameters at the spindle-holder and holder - tool interfaces [5].

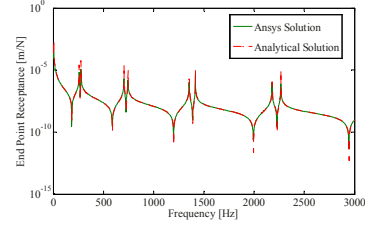


Fig.1. End Point Receptance of a 1m long beam obtained by Ansys and proposed analytical model

Front and rear bearings are also added to the model using structural modification techniques [18]. The coupling procedure is shown in Fig. 2.

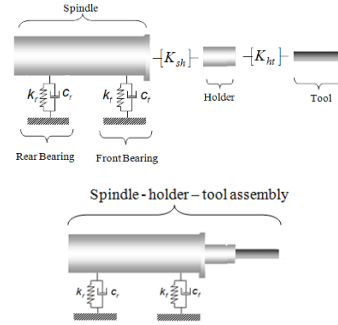


Fig. 2. Spindle Holder Tool assembly

In Fig. 2, k_f and c_f are the linear displacement – to – force stiffness and damping values of the front bearing, respectively; k_r and c_r are linear displacement – to – force stiffness and damping values of the rear bearing, respectively. $[K_{sh}]$ and $[K_{ht}]$ are the contact parameters at the spindle – holder and holder – tool interface, respectively.

2.3 Contact parameters

In dynamic modeling of the spindle-holder-tool assembly the contact parameters play a crucial role [6]. Since there is no theoretical model for obtaining these parameters, Orkun et al. [19] proposed an experimental identification procedure. The identified parameters were used to construct an artificial neural network [20], so that for different spindle, holder and tool combinations, contact parameters can be predicted.

2.4 Bearing parameters

Bearing properties mainly affect the spindle modes of a machine center [7]. During cutting, centrifugal and gyroscopic forces acting on bearings may lead to decrease

in their stiffness [9]. In order to determine these variations of bearing properties, Li and Shin [11] proposed a thermo mechanical model. In a recent study, Orkun et al. [21] used spectral measurement techniques to identify the bearing properties during cutting. Their results showed that bearing properties change significantly during cutting. Thus, variation in the bearing dynamics should also be considered for accurate predictions of FRFs under operational conditions.

3. Case Studies and results

In order to investigate the variation of the tool point FRF under operational conditions several cases are presented in this section.

3.1 Effect of gyroscopic forces

A spindle-holder-tool assembly given by the authors [6] is modeled with the proposed Timoshenko beam model for 30 000 rpm spindle speed. The subassembly FRFs are coupled with receptance coupling method using the translational and rotational stiffness at the holder-tool interface as 2.5×10^7 N/m and 1.5×10^6 N/rad, respectively. The stiffness for the front and rear bearings are taken as 7.5×10^5 N/m and 2.5×10^6 N/m, respectively. The calculated tool point FRF presented in Fig. 3 shows that the spindle modes located at 64 Hz and 190 Hz are not affected by the gyroscopic terms whereas there is a small variation in the tool modes.

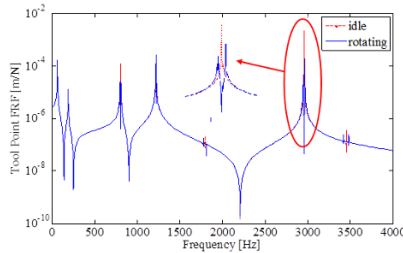


Fig. 3. Tool point FRFs for idle state and at 30000 rpm.

In order to investigate the effect of the contact parameters on the tool point FRF variation, the translational and rotational stiffness at the holder-tool interface is increased to 7.5×10^7 N/m and 7.5×10^6 N/rad, respectively. The predicted tool point FRFs at 30000 rpm given in Fig. 4 which indicates that more stiff connection at the holder-tool interface causes separation of the backward and forward modes at the third and fourth tool modes and the gyroscopic effects become more crucial. The contact parameters also affect the tool modes. Thus, accurate identification of the contact parameters becomes an important key point in the prediction of the tool point FRF in operation.

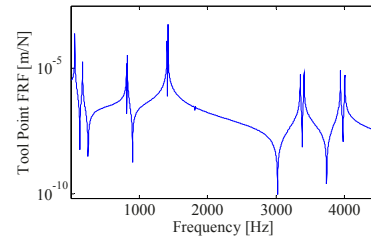


Fig. 4. Tool point FRFs at 30 000 rpm for stiffer connection

3.2 Effect of variations in the bearing properties

The variation of the bearing parameters during operation were identified using the milling force and vibration signals at different speeds [21]. In order to investigate the effects of bearing parameter changes during operation, the tool point FRF is calculated using the bearing properties the idle (5×10^7 N/m and 8×10^7 N/m for the front and rear bearings, respectively), and operating conditions. Assuming similar speed dependent behavior given in references [11, 21], the bearing properties are updated for the rotating case as 4×10^7 N/m and 6×10^7 N/m for the front and rear bearings, respectively 5000 rpm. The FRFs for both cases are shown in Fig. 5. As seen from Fig. 5, with the updated bearing properties even at a moderate speed of 5000 rpm, the variation of the bearing properties causes significant changes in the spindle modes.

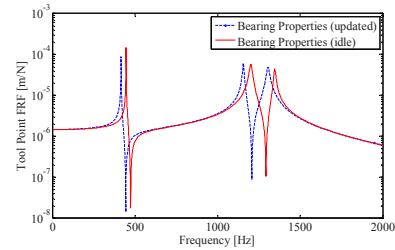


Fig. 5. Tool point FRF variation due to the variation of the bearing properties.

4. Conclusion

In this paper, a complete model for the dynamics of spindle-holder-tool assembly on machining centers under operational conditions is presented. This is done by extending the model developed by the authors for the idle state of the machine to the operational conditions. First a new solution procedure for the rotating Timoshenko beam is proposed and used for the modeling of spindle, holder and tool subassemblies. Obtained subassembly FRFs are coupled using the receptance coupling method with the contact parameters, and the bearing properties are added using the structural modification techniques. Finally, the tool point FRF is obtained for the operational conditions.

Using the analytical modeling approach presented the effects of the gyroscopic moments, contact parameters and bearing parameter variations on the tool point FRF are investigated. Results show that, variations in the structural dynamics due to the gyroscopic moment have negligible effects on the tool point FRF for the case studied. However when the contact parameters of the interface dynamics change, gyroscopic effects become more important. In addition, the effect of the speed dependent bearing parameters on the tool point FRF is investigated and it is observed that the variation in the bearing properties causes significant changes in the spindle modes, and thus in the stability diagrams. Therefore, accurate modeling of the speed dependent bearing properties plays a crucial role in the chatter stability prediction.

References

- [1] Tlustý, J., Poláček M., The stability of machine tools against self-excited vibrations in machining, (1963) Proceedings of the ASME International Research in Production Engineering, Pittsburgh, USA, 465-474
- [2] Altintas Y., Budak, E., (1995) Analytical prediction of stability lobes in milling, *Annals of the CIRP*, 44:357-362
- [3] Budak E., Altintas Y., (1998) Analytical prediction of chatter stability in milling – part I: general formulation; part II: application to common milling systems, *Transactions of ASME, Journal of Dynamic Systems, Measurement, and Control*, 120:22-36
- [4] Schmitz T., Donaldson R., (2000) Predicting high-speed machining dynamics by substructure analysis, *Annals of the CIRP* 49: 303-308
- [5] Ertürk A., Özgüven H.N., Budak E., (2006) Analytical modeling of spindle-tool dynamics on machine tools using Timoshenko beam model and receptance coupling for the prediction of tool point FRF, *International Journal of Machine Tools and Manufacture* 46: 1901-1912
- [6] Ertürk A., Özgüven H.N., Budak E., (2007) Selection of design and operational parameters in spindle-holder-tool assemblies for maximum chatter stability by using a new analytical model, *International Journal of Machine Tools and Manufacture* 47:1401-1409
- [7] Tatar, K., Gren, P., (2007) Measurement of milling tool vibrations during cutting using laser vibrometry, *International Journal of Machine Tools and Manufacture*, 48:380-387
- [8] Zaghbani, I., Songmene, V., (2009) Estimation of machine-tool dynamic parameters during machining operation through operational modal analysis, *International Journal of Machine Tools and Manufacture*, 49:947-957
- [9] Rivin, E., (1999) *Stiffness and Damping in Mechanical Design*, N.Y., USA, Marcel Dekker Inc
- [10] Stone B. J., (1982) The state of the art in the measurement of the stiffness and damping of rolling element bearings, *CIRP Annals Manufacturing Technology*, 31:529-538
- [11] Li, H. Shin Y. C., (2004) Analysis of bearing configuration effects on high speed spindles using an integrated dynamic thermo-mechanical spindle model, *International Journal of Machine Tools & Manufacture*, 44:347-364
- [12] Xiong, G. L., Yi, J. M., Zeng, C., Guo, H. K., Li, L. X., (2003) Study of gyroscopic effect of the spindle on the stability characteristics of the milling system, *Journal of materials Processing Technology*, 138:379-384
- [13] Movahhedy, M. R., Mosaddegh, P., (2006) Prediction of chatter in high speed milling including gyroscopic effects, *International Journal of Machine Tools & Manufacture*, 46: 996-1001
- [14] Aristizabal-Ochoa J.D., (2004) Timoshenko beam-column with generalized end conditions and nonclassical modes of vibration of shear beams, *Journal of Engineering Mechanics* 130:1151–1159
- [15] Wang W., Kirkhope J., (1994) New eigensolutions and modal analysis for gyroscopic/rotor systems Part 1, *Journal of Sound and Vibration*, 175(2):159-170
- [16] Lee C. W., Katz R., Ulsoy A. G., R. A. Scott, (1988) Modal analysis of a distributed parameter rotating shaft, *Journal of Sound and Vibration*, 122(1):119-130
- [17] Lee C. W., Jei Y. G., (1988) Modal analysis of continuous rotor-bearing systems, *Journal of Sound and Vibration*, 126(2):345-361
- [18] Ozguven H.N., (1990) Structural modifications using frequency response functions *Mechanical Systems and Signal Processing* 4 (1):53-63
- [19] Özşahin O., Ertürk A., Özgüven H. N., Budak E., (2009) A closed-form approach for identification of dynamical contact parameters in spindle-holder-tool assemblies, *International Journal of Machine Tools and Manufacture*, 49:25-35
- [20] Özşahin O., Budak E., Özgüven H. N., (2008) Estimation of Dynamic Contact Parameters for Machine Tool Spindle-Holder-Tool Assemblies Using Artificial Neural Networks, *Proceedings of the 3rd International Conference on Manufacturing Engineering (ICMEN)*, pp. 131-144
- [21] Özşahin O., Budak E., Özgüven H. N., (2011) Investigating dynamics of machine tool spindles under operational conditions, *13th CIRP Conference on modeling of machining operations*